



Stepwise Oligocene–Miocene breakdown of subpolar gyres and strengthening of the Antarctic Circumpolar Current

Frida S. Hoem^{1,a}, Karlijn van den Broek¹, Adrián López-Quirós², Suzanna H. A. van de Lagemaat¹,
Steve M. Bohaty^{3,b}, Claus-Dieter Hillenbrand⁴, Robert D. Larter⁴, Tim E. van Peer^{3,5,c},
Henk Brinkhuis^{1,6}, Francesca Sangiorgi¹, and Peter K. Bijl¹

¹Department of Earth Science, Utrecht University, Utrecht, the Netherlands

²Department of Stratigraphy and Paleontology, University of Granada, Granada, Spain

³School of Ocean and Earth Science, National Oceanography Centre Southampton,
University of Southampton, Southampton, UK

⁴British Antarctic Survey, Cambridge, UK

⁵Department of Earth Sciences, University College London, London, UK

⁶Department of Ocean Systems Research, Royal Netherlands Institute for Sea Research (NIOZ),
Texel, the Netherlands

^anow at: Department of Earth Science, University of Bergen, Bergen, Norway

^bnow at: Institute of Earth Sciences, Heidelberg University, Heidelberg, Germany

^cnow at: School of Geography, Geology and the Environment, University of Leicester, Leicester, UK

Correspondence: Frida S. Hoem (frida.hoem@uib.no)

Received: 6 October 2023 – Revised: 27 August 2024 – Published: 19 December 2024

Abstract. Through the Cenozoic (66–0 Ma), the dominant mode of ocean surface circulation in the Southern Ocean transitioned from two large subpolar gyres to circumpolar circulation with a strong Antarctic Circumpolar Current (ACC) and complex ocean frontal system. Recent investigations in the southern Indian and Pacific oceans show warm Oligocene surface water conditions with weak frontal systems that started to strengthen and migrate northwards during the late Oligocene. However, due to the paucity of sedimentary records and regional challenges with traditional proxy methods, questions remain about the southern Atlantic oceanographic transition from gyral to circumpolar circulation, with associated development of frontal systems and sea ice cover in the Weddell Sea. Our ability to reconstruct past Southern Ocean surface circulation and the dynamic latitudinal positions of the frontal systems has improved over the past decade. Specifically, increased understanding of the modern ecologic affinity of organic-walled dinoflagellate cyst (dinocyst) assemblages from the Southern Ocean has improved reconstructions of distinct past oceanographic conditions (sea surface temperature, salinity, nutrients, and sea ice) using downcore assemblages from marine sediment records. Here we present new late Oligocene to latest Miocene (~26–5 Ma) dinocyst assemblage data from marine sediment cores in the southwestern Atlantic Ocean (International Ocean Discovery Program (IODP) Site U1536, Ocean Drilling Program (ODP) Site 696 and piston cores from Maurice Ewing Bank). We compare these to previously published latest Eocene–latest Miocene (~37–5 Ma) dinocyst assemblage records and sea surface temperature (SST) reconstructions available from the SW Atlantic Ocean in order to reveal oceanographic changes as the Southern Ocean gateways widen and deepen. The observed dinocyst assemblage changes across the latitudes suggest a progressive retraction of the subpolar gyre and southward migration of the subtropical gyre in the Oligocene–early Miocene, with strengthening of frontal systems and progressive cooling since the middle Miocene (~14 Ma). Our data are in line with the timing of the removal of bathymetric and geographic obstructions in the Drake Passage and Tasmanian Gateway regions, which enhanced deep-water throughflow that broke down gyral circulation into the

Antarctic circumpolar flow. Although the geographic and temporal coverage of the data is relatively limited, they provide a first insight into the surface oceanographic evolution of the late Cenozoic southern Atlantic Ocean.

1 Introduction

Today, the Southern Ocean is known for hosting the strongest surface ocean current on Earth: the mainly wind-driven, eastward-flowing Antarctic Circumpolar Current (ACC), which connects the southern Indian, Pacific and Atlantic oceans. This current system is characterized by a strong latitudinal temperature gradient and associated changes in oceanographic conditions along five frontal systems: the Subtropical Front (STF), the Subantarctic Front (SAF), the Polar Front (PF), the Southern ACC Front (sACCf), and the Southern Boundary (sBdy) of the ACC (e.g. Orsi et al., 1995; Fig. 1). In the early Cenozoic (66–34 Ma), southern high-latitude ocean circulation was dominated by two large subpolar gyres (Huber et al., 2004; Sijp and England, 2004; Bijl et al., 2011; Sijp et al., 2016). This gyral circulation broke down during the late Cenozoic, when a throughflow developed, mostly enabled by the opening and deepening of the Southern Ocean gateways (Kennett, 1977; Sauermilch et al., 2021). While the Tasmanian Gateway deepened between 35.5 and 33.5 Ma (Stickley et al., 2004) and widened between 33 and 30 Ma (Scher et al., 2015), the timing and nature of the opening, widening, and deepening of the Drake Passage remains elusive with age estimates of a deep opening ranging from the Eocene to earliest Miocene (Barker and Burrell, 1977; Barker et al., 2007; Livermore et al., 2007; Lagabrielle et al., 2009; Eagles and Jokat, 2014; Maldonado et al., 2014; van de Lagemaat et al., 2021). The most recent research (Evangelinos et al., 2024) estimates that the modern, vigorous, and deep-reaching ACC developed some time in the late Miocene and reduced the size of the once large subpolar gyres into comparatively small gyres in the Weddell Sea and the Ross Sea today.

In the absence of calcareous (and often even siliceous) microfossils in Cenozoic Southern Ocean sediments, studies from the southern Pacific and southern Indian oceans have successfully utilized organic components preserved in these sedimentary archives. Notably, investigations of the remains of dinoflagellates (their organic cysts) and molecular organic geochemical analyses are employed to reconstruct the Oligocene–Miocene evolution of oceanic conditions, temperature gradients, and paleo-positions of frontal systems in the Southern Ocean (Hannah, 2006; Lyle et al., 2007; Guerstein et al., 2010; Houben et al., 2013; Prebble et al., 2013; Scher et al., 2015; Warny et al., 2016; Hartman et al., 2018; Sangiorgi et al., 2018; Bijl et al., 2018a; Evangelinos et al., 2020; Parras et al., 2020; Hoem et al., 2021a, b; Amenábar et al., 2022; Duncan et al., 2022; Hou et al., 2023). The Oligocene record of Integrated Ocean Drilling Program

(IODP) Site U1356 offshore Wilkes Land (Bijl et al., 2018a; Hartman et al., 2018) and Deep Sea Drilling Project (DSDP) Site 274 offshore from the Ross Sea embayment (Hoem et al., 2021a) show surprisingly warm (10–21 °C) sea surface temperatures (SSTs) and dinoflagellate cyst (dinocyst) assemblages, which indicate oligotrophic, fully marine, and temperate waters in areas proximal to the East Antarctic Ice Sheet. Across the Australo-Antarctic Gulf, Oligocene SST records show a relatively small temperature gradient (~6–8 °C) between the STF (Ocean Drilling Program (ODP) Site 1168) and the Antarctic margin (IODP Site U1356). This SST gradient increased (> 10 °C) from ~26 Ma onwards due to an SST decrease proximal to the Antarctic continent (Hartman et al., 2018; Duncan et al., 2022), while SSTs south of Australia remained high (Hoem et al., 2022). The cooling close to Antarctica was attributed to the first deep opening of Drake Passage (van de Lagemaat et al., 2021), causing a stronger circum-Antarctic throughflow, weakening the gyre circulation and increasing the thermal isolation of Antarctica (Sauermilch et al., 2021; Hoem et al., 2022). Mid-latitude warmth in the early to middle Miocene was followed by a gradual but profound 10 °C cooling in the middle to late Miocene (Herbert et al., 2016; Hou et al., 2022). Although several reconstructions indicate surface ocean conditions from the southern Atlantic across the Eocene and the Eocene–Oligocene Transition (EOT) (Douglas et al., 2014; Plancq et al., 2014; Houben et al., 2019; Bijl et al., 2021; Amenábar et al., 2022; Tibbett et al., 2022; Guerstein et al., 2008, 2014, 2023; Premaor et al., 2023), Oligocene and Miocene data from the southern Atlantic are sparse (Hoem et al., 2023). Hoem et al. (2023) used organic biomarkers (TEX₈₆) to reconstruct the late Eocene–early Oligocene and middle–late Miocene SST gradient in the southern Atlantic, and while this demonstrated an increase in the temperature gradient in the southern Atlantic, questions remain about the development and positions of ocean frontal systems and whether sea ice was present.

Dinocyst assemblage analysis allows tracing the positions of oceanic fronts and frontal zones, each of which is characterized by specific environmental surface water conditions and thus habitat preference for dinoflagellates (Thöle et al., 2023). These biogeographic reconstructions use established relationships between modern dinocysts from core top sediments (predominantly from box cores) and environmental conditions in the upper surface waters, such as temperature, concentration of nutrients, upwelling intensity, salinity, and sea ice cover (Prebble et al., 2013; Zonneveld et al., 2013; Marret et al., 2020; Thöle et al., 2023). Many modern dinocysts have long lineages in the Southern Ocean (Bijl,

2022) dating back to the Oligocene. Although a few species have shown changes in their ecological preference through time (De Schepper et al., 2011), we assume that the ecological niche of the majority of Oligocene and Miocene dinoflagellate species, which are still living in the modern ocean, is the same or similar (e.g. Hou et al., 2023). We then use these organic microfossil remains (dinocysts) to track past changes in surface ocean conditions, fronts, and currents.

In this study, we reconstruct the late Eocene–Miocene (35–6 Ma) oceanographic evolution of the southern Atlantic region through dinocyst assemblage analysis of sediment drill cores from the northwestern Weddell Sea (ODP Site 696) and Scotia Sea (International Ocean Drilling Program (IODP) Site U1536) and piston cores obtained during a recent marine geological and geophysical cruise to the Maurice Ewing Bank (RRS *Discovery* Expedition DY087; cores DY087-15PC and DY087-09PC), integrated with existing southern Atlantic dinocyst records (stars in Fig. 1). In conjunction with using organic paleothermometry (TEX₈₆) data for reconstructing SSTs (Hoem et al., 2023), we aim to reconstruct the surface ocean properties, including the geographical positions of fronts and gyres, to identify the role of the deepening of the Drake Passage for climatic cooling and Antarctic Ice Sheet expansion and for southern Atlantic oceanography in the late Eocene–Miocene.

2 Material

2.1 DY087 piston cores

We studied sediments from two piston cores collected from the southeastern flank of Maurice Ewing Bank in the southwestern Atlantic Ocean during RRS *Discovery* cruise DY087 (January–March 2018): core DY087-09PC (recovery: 3.36 m) retrieved at 50°17.18′ S and 42°27.32′ W from a water depth of 1351 m and core DY087-15PC (recovery: 2.39 m) retrieved at 50°11.60′ S and 42°32.72′ W from a water depth of 1430 m. In the modern ocean, Circumpolar Deep Water sweeps across the shallower areas of Maurice Ewing Bank (~ 500–3000 m) and northwards along the base of its eastern slope (Garabato et al., 2002). As a consequence of this strong current activity, erosion on the bank exposed Miocene and older strata (Ciesielski and Wise, 1977; Ciesielski et al., 1982). Sub-bottom profiler data (Fig. 2a) and preliminary biostratigraphic data from the piston cores indicate that sediment deposition on Maurice Ewing Bank has been influenced by bottom currents since the Oligocene, as is evident from various packages of drift deposits with non-conformable erosive bases.

Several hiatus-bound sediment packages seen in the sub-bottom profiler data (coloured lines, Fig. 2b) likely reflect changes in the mode of ocean currents in the region. The interpretations of both the acoustic sub-bottom profile and a simultaneously collected seismic reflection profile are subjects of parallel studies (Tim E. van Peer, personal commu-

nication, 8 December 2023). The sub-bottom profile along multichannel seismic profile L20A (Fig. 2) reveals that the strata sampled in core DY087-15PC (indicated by red reflectors in Fig. 2b) do not extend to site DY087-09PC but rather are unconformably overlain by younger strata (above the blue reflector). Core DY087-15PC recovered an apparently current-winnowed sandy to gravelly top unit of diatomaceous sediments (0–58 cm depth) with abundant planktic foraminifera in the uppermost 13 cm. The underlying sedimentary sequence consists of bioturbated to structureless diatomaceous ooze (58–208 cm) and diatomaceous nannofossil ooze (208–239 cm). Core DY087-09PC retrieved a similar, obviously current-winnowed top unit of sandy to gravelly diatomaceous sediments (0–46 cm), which contain abundant planktic foraminifera near the core surface (0–9 cm). This top unit is underlain by partly bioturbated and crudely laminated to stratified diatom-bearing to diatomaceous nannofossil ooze (46–336 cm), which is sandy below 163 cm core depth.

2.2 ODP Site 696

ODP Leg 113 Site 696 was drilled in the northwestern Weddell Sea (61°50.959′ S, 42°55.996′ W, 646 m water depth) on the platform of the South Orkney Microcontinent (Fig. 1), located south of the Southern Boundary of the ACC Front (Barker et al., 1988). The depositional setting at Site 696 is that of shallow marine and coastal environmental conditions in the Eocene, invigorated bottom water circulation in the latest Eocene–earliest Oligocene and continued deepening of the South Orkney Microcontinent shelf and full separation from the Antarctic Peninsula in the Miocene (Barker et al., 1988; Houben et al., 2019; López-Quirós et al., 2021). Building on the section dated to the Eocene to earliest Oligocene (Cores 59R–53R) studied by Houben et al. (2019), we extend the palynological record at ODP Site 696 up-core from 548.9 to 520.6 m below the seafloor (m b.s.f.) (Cores 52R–50R) and discuss recent age model modifications for this upper interval. The lithology of the studied interval above the claystone and clayey mudstones of earliest Oligocene age (Core 53R) consists of rhythmically interbedded sandy mudstones with glauconite-bearing sandstone beds (548.9–529.8 m b.s.f., Core 52R, Core 51R), which were likely deposited by bottom currents and in some instances possibly as slumps (López-Quirós et al., 2020). At the top of Core 51R (529 m b.s.f.), sharp contact between glauconite-bearing sandstone and overlying muddy diatomaceous ooze recovered in Core 50R (522–520.6 m b.s.f.) likely represents a break in sedimentation (hiatus).

2.3 IODP Site U1536

IODP Expedition 382 Site U1536 was drilled in Dove Basin in the southern Scotia Sea (59°26.4608′ S, 41°3.6399′ W, 3220 m water depth; Weber et al., 2021). Sediments in Dove

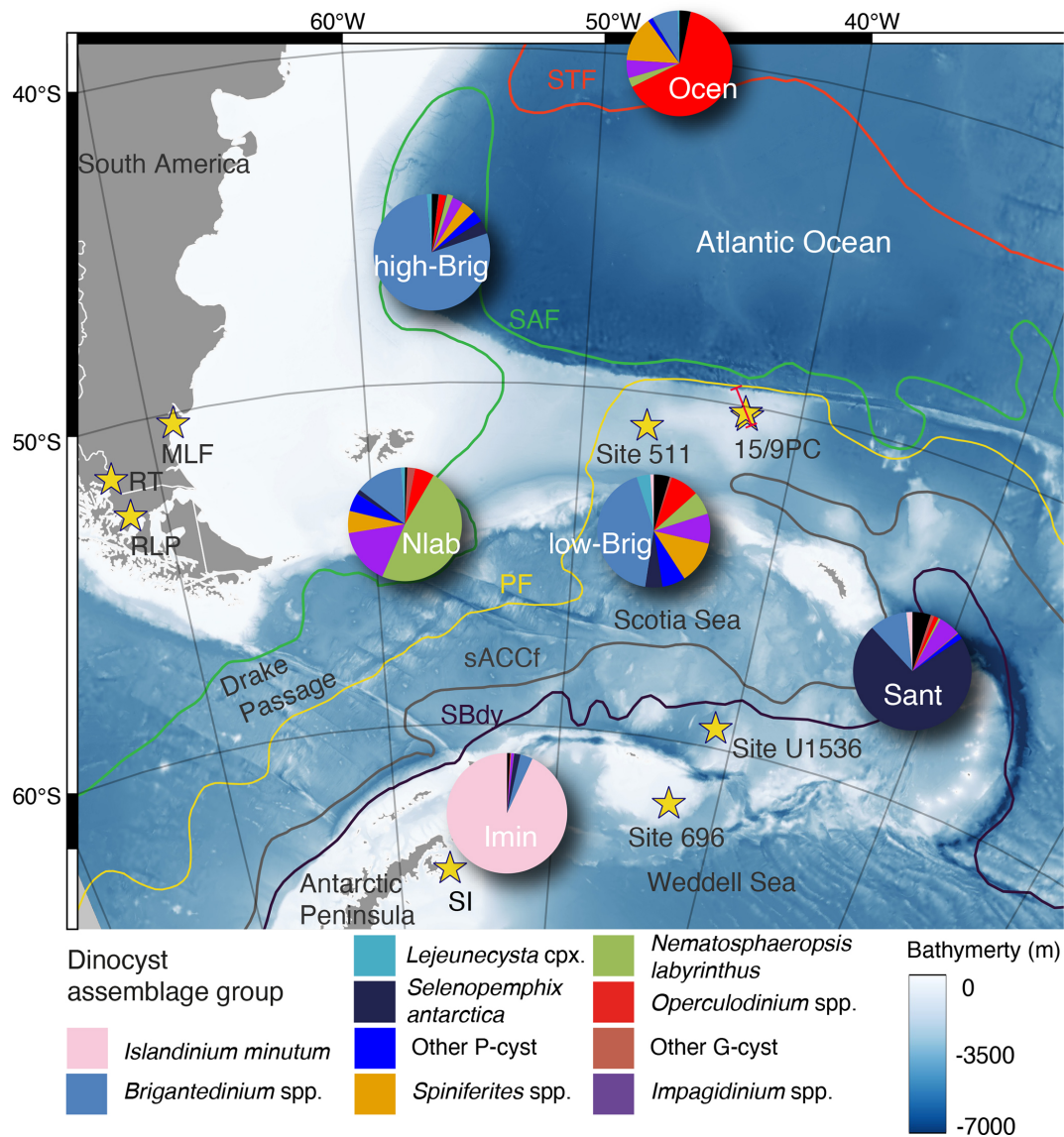


Figure 1. Modern locations of the sites investigated and discussed in this study (yellow stars). SI is Seymour Island, RLP is Río Los Palos, RT is Río Turbio, and MLF is the Monte León Formation. Grey areas outline modern land areas and grounded ice. The blue gradient colour in the map shows the southern Atlantic bathymetry according to the General Bathymetric Chart of the Oceans (GEBCO, 2023; last access: 1 August 2023). The coloured lines depict the smoothed average positions of circumpolar fronts (Orsi et al., 1995): the Subtropical Front (STF), the Subantarctic Front (SAF), the Polar Front (PF), the Southern ACC Front (sACCf), and the Southern Boundary of the ACC Front (SBdy). The red line across sites (DY087) 15PC and 9PC shows the location of an acoustic sub-bottom profile presented in Fig. 2. The pie charts show the present-day southern Atlantic dinocyst assemblage distribution clusters, derived from surface ocean data compiled by Thöle et al. (2023) and discussed here in Sect. 3.2.

Basin are primarily deposited by contourite currents along the bottom-current pathway of the ACC and northward-flowing Weddell Sea Deep Water, as well as pelagic aggregates (generated mainly by diatom productivity, aeolian dust, and iceberg-rafted debris deposition) and tectonically induced downslope transport (Garabato et al., 2002; Weber et al., 2021; Pérez et al., 2021). The lithology of the studied interval from the sediment record of Hole U1536E from

640–460 m b.s.f. (Cores 33R–15R) consists of silty clays interbedded with diatomaceous ooze, with sparse fragments of lithified mudstone and gravel conglomerate–breccia in cores retrieved below a prominent seismic reflector at 566 m b.s.f., referred to as “Reflector-c” (Pérez et al., 2021). The sediments recovered below this depth are affected by moderate to high drilling disturbance, such as biscuiting or brecciation of core material caused by rotary drilling and compaction of

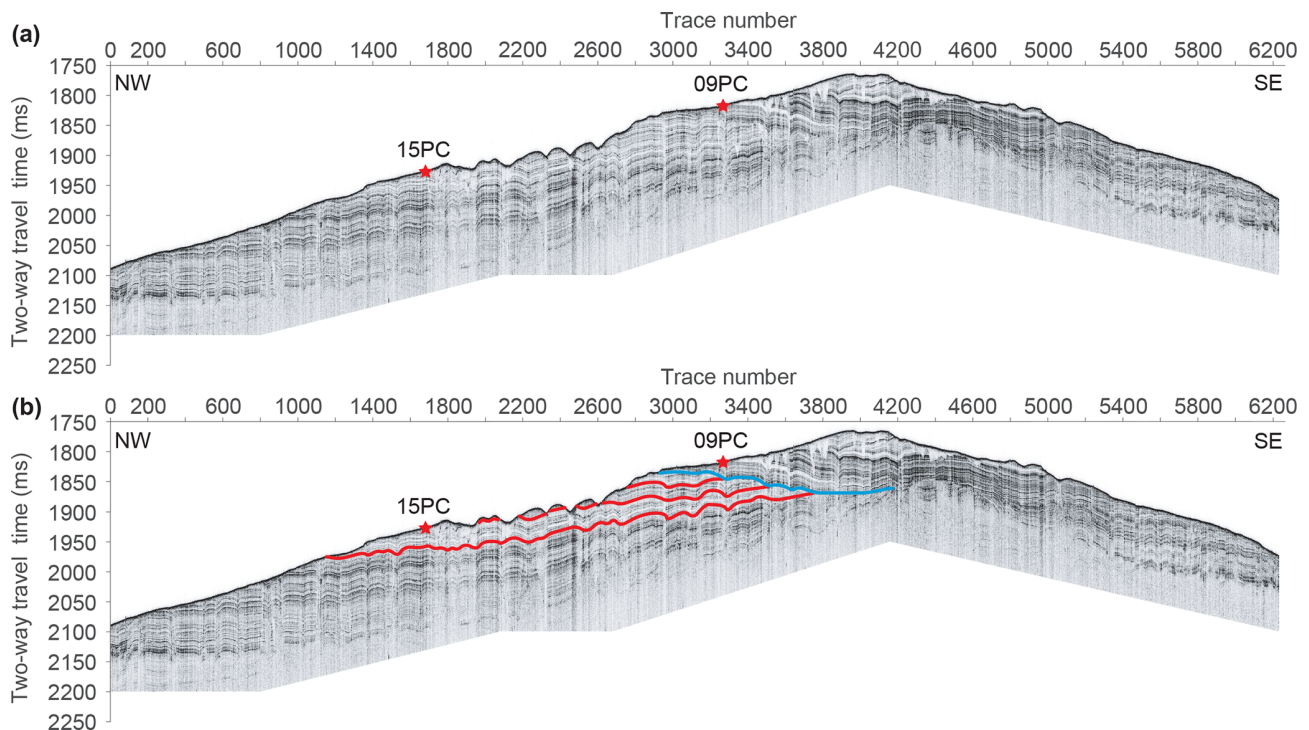


Figure 2. Acoustic sub-bottom profile collected along multichannel seismic profile L20A on cruise DY087. **(a)** Original data. **(b)** Interpretation of seismic reflections (red and blue lines) and locations of cores 15PC and 09PC.

gravel-rich material. Based on the shipboard biostratigraphic and magnetostratigraphic age model (Weber et al., 2021), which we follow here, the sediments at 480–450 m b.s.f. depth (Cores 16R–13R) have an age of 6–5 Ma, and those at 548–535 m b.s.f. depth (Cores 24R–22R) have an age of 7.7–6.4 Ma. Seismic interpretations by Pérez et al. (2021) in combination with shipboard biostratigraphy (Weber et al., 2021) assigned an age of ~ 8.4 Ma to the sediments at 617–566 m b.s.f. depth (Cores 30R–26R) above Reflector-c, and an age of ~ 14.2 Ma to the sediments at 622 m b.s.f. depth (Core 31R) below Reflector-c. Since no sediments from the interval spanning Reflector-c were recovered, it is possible that Reflector-c represents a prolonged time interval of condensed sedimentation, non-deposition, or erosion.

3 Methods

3.1 Palynological processing and analysis

Palynological processing followed standard procedures at GeoLab, Utrecht University, as described in Hoem et al. (2021a). In short, 10–15 g of dried sediment samples were digested using cold hydrochloric and hydrofluoric acid and spiked with *Lycopodium clavatum* spores ($n = 9666 \pm 213$). The palynological residues were then sieved through a 10 μm nylon mesh aided by an ultrasonic bath, mounted on glass slides using glycerine jelly, sealed with nail varnish, and counted (under 400 \times magnification) using a transmitted light

optical microscope. Dinocyst taxonomy follows that cited in Williams et al. (2017) and Clowes et al. (2016) and informal species as presented in Bijl et al. (2018b).

3.2 Ecological affinities of dinocyst species

Under the assumption that the habitat affinities and feeding strategies of extant dinoflagellate species were similar in the past, we employ dinocyst assemblages as a paleoenvironmental proxy to reconstruct upper-water-column changes through the late Eocene, Oligocene, and Miocene in the SW Atlantic Ocean. Distributions of dinocysts in the present ocean and their preservation in underlying seafloor sediments are controlled by various factors, mainly surface water temperature but also nutrient availability, salinity, bottom water oxygen concentration, sea ice cover, and transport by surface to deep-ocean currents (Dale, 1996; Prebble et al., 2013; Zonneveld et al., 2013) (Table 1). Most modern Antarctic dinocysts belong to either the gonyaulacoid (G) or the (proto-)peridinioid (P) dinoflagellates. P-(dino)cysts are today mostly produced by heterotrophic dinoflagellates and are mainly found in and below nutrient-rich environments, like river plumes, upwelling areas, and (perennial) sea ice zones (Zonneveld et al., 2013). They currently dominate the southern high-latitude dinocyst assemblages south of the SAF (Zonneveld et al., 2013; Thöle et al., 2023), while the cysts produced by phototrophic and mixotrophic G-dinoflagellates dominate in temperate waters in a broad range of trophic con-

Table 1. Dinocyst assemblage groups and ecological affinities.

Dinocyst assemblage group	Species included	Ecological affinity	References
<i>Lejeunecysta</i> cpx	<i>Lejeunecysta</i> spp., <i>Selenopemphix</i> spp., <i>Malvinia escutiana</i> , <i>Protoperidinium</i> spp.	High productivity	Harland and Pudsey (1999); Sluijs et al. (2003); Zonneveld et al. (2013)
<i>Brigantedinium</i> spp.	<i>Brigantedinium</i> simplex, <i>B. pynei</i> , <i>B. sp. A</i> , <i>B. sp. B</i> (Houben et al., 2019)	High productivity	Zonneveld et al. (2013)
<i>Selenopemphix antarctica</i>	<i>S. antarctica</i>	High productivity, cool waters, sea ice presence	Thöle et al. (2023)
Other P-cysts	<i>Alterbidinium distinctum</i> , <i>Deflandrea</i> spp., <i>Octodinium askiniae</i> , <i>Senegalinium</i> spp., <i>Protoperidinium</i> spp.	High productivity	Harland and Pudsey (1999); Sluijs et al. (2003); Zonneveld et al. (2013)
<i>Spinidinium</i> cpx.	<i>Spinidinium</i> spp., <i>Moria zachosii</i> , <i>Vozzhennikovia</i> spp.	High productivity, high terrestrial runoff, tolerant of low salinity	Sluijs and Brinkhuis (2009)
<i>Spiniferites</i> spp.	<i>Spiniferites</i> spp.	Low nutrients, open marine, north of the STF, warm water	Brinkhuis (1994); Zonneveld et al. (2013); Thöle et al. (2023)
<i>Impagidinium</i> spp.	<i>Impagidinium pallidum</i> , <i>I. aculeatum</i> , <i>I. velorum</i> , <i>I. patulum</i>	Oligotrophic (open) oceanic <i>I. pallidum</i> is found in polar, low-salinity (meltwater), open-ocean regions today	Wall et al. (1977); Pross and Brinkhuis (2005); De Schepper et al. (2011); Zonneveld et al. (2013)
<i>Nematosphaeropsis labyrinthus</i>	<i>Nematosphaeropsis labyrinthus</i>	Oceanic, south of the STF	Crouch et al. (2010); Prebble et al. (2013)
<i>Operculodinium</i> spp.	<i>Operculodinium centrocarpum</i> , <i>O. janduchenei</i>	Cosmopolitan or oceanic, abundant north of the STF	Brinkhuis et al. (1994); Prebble et al. (2013)
Other G-cysts	<i>Gelatia inflata</i> , <i>Invertocysta tabulata</i> , <i>Achomospaera allicornu</i> , <i>Hystriochokolpoma</i> cf. <i>rigaudiae</i> , <i>Cerebrocysta</i> spp., <i>Corrudinium</i> spp., <i>Pyxidinosia</i> spp., <i>Batiacasphaera</i> spp., <i>Samlandia chlamydotheca</i> , <i>Chiropteridium galea</i> , <i>Enneadocysta</i> spp.	Oceanic, neritic	Brinkhuis (1994); Sluijs et al. (2005)
<i>Phthanoperidinium</i> spp.	<i>Phthanoperidinium</i> sp. C, <i>P. stockmansii</i>	High productivity, tolerant of low salinity	Sluijs and Brinkhuis (2009); Barke et al. (2011); Neville et al. (2019)
<i>Islandinium minutum</i>	<i>I. minutum</i>	High productivity, tolerant of low salinity	Thöle et al. (2023)

ditions. These gonyaulacoid taxa (G-cysts) are rare to absent in close proximity to the Antarctic Ice Sheet and in regions where sea ice is present throughout most of the year (Prebble et al., 2013). Today, a pronounced latitudinal separation of dinocyst assemblages exists across the southern Atlantic and its fronts (Esper and Zonneveld, 2002; Prebble et al., 2013; Marret et al., 2020; Thöle et al., 2023) (Fig. 1). This marked

dinocyst biogeographic distribution pattern makes dinocysts promising tracers of past frontal system movements. Seafloor surface sediment samples from south of the SAF, where mixing and upwelling of cold, nutrient-rich waters occur, and south of the PF, where strong seasonality in sea ice cover occurs, contain assemblages overwhelmingly dominated by peridinioid and protoperidinioid taxa (collectively referred

to as P-cysts) produced by heterotrophic taxa (Fig. 1). Surface sediment samples to the east of the northern Antarctic Peninsula are dominated by *Islandinium minutum*, indicative of cold freshwater associated with iceberg discharge and melting (Cluster Imin in Thöle et al., 2023; see also Head et al., 2001). At the sBdy in the southern Scotia Sea, assemblages in seafloor surface sediments are dominated by the sea-ice-affiliated dinocyst *Selenopemphix antarctica* (Cluster Sant in Thöle et al., 2023; see also Harland and Pudsey, 1999; Zonneveld et al., 2013; Marret et al., 2020). South of the PF, the assemblages in core top sediments contain abundant *Brigantedinium* spp. produced by heterotrophic taxa, which indicates presence of nutrient-rich waters due to mixing and upwelling (Cluster low-Brig in Thöle et al., 2023) but not necessarily influenced by sea ice, as well as common open-ocean cosmopolitan species. *Nematosphaeropsis labyrinthus* is typical of the modern subantarctic zone (Cluster Nlab in Thöle et al., 2023) between the SAF and STF. At the eastern continental margin of South America, surface sediment samples are dominated by *Brigantedinium* spp., indicating mixing and upwelling and potentially high nutrient input from eastern South America (Cluster high-Brig in Thöle et al., 2023). In the open ocean, for warmer water settings north of the STF, seafloor surface samples are dominated by the autotrophic cosmopolitan gonyaulacoid species *Operculodinium* spp., accompanied by *Spiniferites* spp. (Cluster Ocen) and *Pyxidinosia* spp. Several *Impagidinium* species (*Impagidinium velorum*, *Impagidinium patulum*, and *Impagidinium aculeatum*) are also found at locations north of the STF. These species are the cysts of taxa thriving in open ocean, low-productivity or oligotrophic environments, and *Impagidinium aculeatum* in particular is a species indicative of warm-water conditions (Zonneveld et al., 2013). An exception is *Impagidinium pallidum*, which is abundantly recorded in both polar areas in the modern ocean (Zonneveld et al., 2013; Marret et al., 2020) but is present in the warm Miocene record off Wilkes Land (Sangiorgi et al., 2018) and also recorded in temperate waters during the Neogene (De Schepper et al., 2011). Therefore, we interpret the paleoecological signal of *Impagidinium pallidum* in the past with caution (De Schepper et al., 2011).

The ecological preferences of extinct dinocyst taxa cannot be directly correlated to modern affinities. As an alternative, the paleoecological conditions that these extinct species represent have been inferred from their co-occurrence with extant species for which the ecological information is available (e.g. Schreck and Matthiessen, 2013) or other paleoceanographic proxies for temperature, freshwater runoff and input, and nutrient conditions analysed on the same sediment samples (Bijl et al., 2011; De Schepper et al., 2011; Frieling and Sluijs, 2018) (Table 1). In general, we assume from these empirical studies that extinct P-cyst species had the same heterotrophic lifestyle as their living counterparts, while extinct G-cysts had an autotrophic or mixotrophic behaviour (Sluijs et al., 2005; Esper and Zonneveld, 2007). A distinct group of

dinocyst taxa, among them species of the now extinct P-cyst genera *Spinidinium* spp. and *Vozzhennikovia* spp., had an endemic Antarctic distribution in the Eocene (Guerstein et al., 2008; Bijl et al., 2011). These “Antarctic endemic taxa” track surface currents originating from near the Antarctic coast, while cosmopolitan dinocysts track currents sourced from low latitudes (Huber et al., 2004; Warnaar et al., 2009; Guerstein et al., 2010; Bijl et al., 2011, 2013). The Antarctic endemic taxa that dominated the Eocene Southern Ocean sediments were replaced in the earliest Oligocene by dinocyst assemblages similar to present-day examples (Houben et al., 2013, 2019). High abundances of extinct cosmopolitan species of *Phthanoperidinium* are usually associated with low-salinity, neritic environments characterized by high nutrient supply, e.g. in the Arctic Ocean (Barke et al., 2011; Frieling and Sluijs, 2018; Neville et al., 2019). In the Antarctic, surface water freshening could be induced by high rates of runoff, precipitation, or glacial meltwater supply, including melting of icebergs.

3.3 Diatom processing and biostratigraphy

Smear slides were prepared from selected intervals of Cores DY087-09PC and 15PC for diatom biostratigraphic analysis. The slides were mounted using Norland Optical Adhesive (no. 61) and examined under a transmitted light microscope (at 400× and 1000× magnification). Key diatom species were noted, and biostratigraphic age estimates were determined using a recent age compilation of Southern Ocean diatom events for IODP Exp. 374 studies (McKay et al., 2019).

4 Results

4.1 New and revisited age constraints

4.1.1 DY087-15PC

Diatoms examined from DY087-15PC at depths of 142 and 122 cm conservatively indicate a late Oligocene to earliest Miocene age between 26.4 and 22.7 Ma based on the presence of *Azpeitia gombosi* (first appearance datum (FAD): ~ 28 Ma; last appearance datum (LAD): ~ 20 Ma), *Cavitatus jouseanus* (FAD: 30.6 Ma), *Hemiaulus taurus* (FAD: ~ 28 Ma; LAD: ~ 22–23 Ma), *Rocella gelida* (FAD: 26.4 Ma; LAD: 22.7 Ma), and *Rocella schraderi* (FAD: ~ 26 Ma; LAD: ~ 23 Ma), with the younger age limit supported by the absence of *Thalassiosira spumellaroides* (FAD: 22.7 Ma) and *Thalassiosira praepraga* (FAD: 18.6–20.8 Ma) (Table 2). The two most important dinocyst species constraining the ages of sediments in core DY087-15PC (Fig. 3) are *Invertocysta tabulata* and *Gelatia inflata*. *Invertocysta tabulata* has only been identified in the uppermost sample (100–105 cm), whereas *Gelatia inflata* has been identified in all samples below 105 cm core depth. As *Gelatia inflata* has a biostratigraphic range of 33.7–23.8 Ma and *Invertocysta tabulata* has a range of 23.6–16.5 Ma, the interval between these

Table 2. Diatom and dinocyst biostratigraphic age ranges for sediment samples analysed in piston core DY087-15PC.

Expedition, core, interval	Core depth mean (cm)	Event	Microfossil group	Taxa	Age (Ma) GTS12 (Gradstein et al., 2012)	Reference
DY087, 15PC, 100–105 cm	103	FAD	Dinocyst	<i>Operculodinium janduchenei</i>	24	Bijl et al. (2018b)
DY087, 15PC, 100–105 cm	103	FAD	Dinocyst	<i>Invertocysta tabulata</i>	23.6	Bijl et al. (2018b)
DY087, 15PC, 100–105 cm	103	FAD	Dinocyst	<i>Impagidinium velorum</i>	33.7	Bijl et al. (2018b)
DY087, 15PC, 100–105 cm	103	FAD	Dinocyst	<i>Impagidinium aculeatum</i>	34.4	Bijl et al. (2018b)
DY087, 15PC, 122 and 142 cm	132	LAD	Diatom	<i>Azpeitia gombosi</i>	~ 20	McKay et al. (2019)
DY087, 15PC, 122 and 142 cm	132	LAD	Diatom	<i>Rocella gelida</i>	~ 22.7	McKay et al. (2019)
DY087, 15PC, 122 and 142 cm	132	LAD	Diatom	<i>Hemiaulus taurus</i>	~ 22–23	McKay et al. (2019)
DY087, 15PC, 122 and 142 cm	132	LAD	Diatom	<i>Rocella schraderi</i>	~ 23	McKay et al. (2019)
DY087, 15PC, 122 and 142 cm	132	FAD	Diatom	<i>Rocella schraderi</i>	~ 26	McKay et al. (2019)
DY087, 15PC, 122 and 142 cm	132	FAD	Diatom	<i>Rocella gelida</i>	26.4	Roberts et al. (2003), McKay et al. (2019)
DY087, 15PC, 122 and 142 cm	132	FAD	Diatom	<i>Hemiaulus taurus</i>	~ 28	Harwood and Maruyama (1992), Roberts et al. (2003)
DY087, 15PC, 122 and 142 cm	132	FAD	Diatom	<i>Azpeitia gombosi</i>	~ 28.5	Harwood and Maruyama (1992), Roberts et al. (2003)
DY087, 15PC, 122 and 142 cm	132	FAD	Diatom	<i>Cavitatus jouseanus</i>	30.6	Roberts et al. (2003)
DY087, 15PC, 160–165 cm	163	LAD	Dinocyst	<i>Gelatia inflata</i>	23.8	Bijl et al. (2018b)
DY087, 15PC, 218–223 cm	221	FAD	Dinocyst	<i>Impagidinium patulum</i>	33.7	Bijl et al. (2018b)
DY087, 15PC, 231–236 cm	234	FAD	Dinocyst	<i>Impagidinium pallidum</i>	33.7	Bijl et al. (2018b)
DY087, 15PC, 231–236 cm	234	FAD	Dinocyst	<i>Gelatia inflata</i>	33.7	Bijl et al. (2018b)

Table 3. Diatom and dinocyst biostratigraphic age ranges for sediment samples analysed in piston core DY087-09PC.

Expedition, core, interval	Core depth mean (cm)	Event	Microfossil group	Taxa	Age (Ma) GTS12 (Gradstein et al., 2012)	Reference
DY087, 09PC, 60–65 cm	63	LAD	Dinocyst	<i>Invertocysta tabulata</i>	16.5	Bijl et al. (2018b)
DY087, 09PC, 220 cm	220	FAD	Diatom	<i>Cavitatus miocenicus</i>	24	McKay et al. (2019)
DY087, 09PC, 220 cm	220	FAD	Diatom	<i>Dactyliosolen</i> sp.	~ 26	McKay et al. (2019)
DY087, 09PC, 220 cm	220	LAD	Diatom	<i>Thalassiosira praeфрага</i>	17.4–17.7	Cody et al. (2008)
DY087, 09PC, 220 cm	220	FAD	Diatom	<i>Thalassiosira praeфрага</i>	18.6–20.8	McKay et al. (2019)
DY087, 09PC, 307–312 cm	310	FAD	Dinocyst	<i>Invertocysta tabulata</i>	23.6	Bijl et al. (2018b)
DY087, 09PC, 307–312 cm	310	FAD	Dinocyst	<i>Impagidinium pallidum</i>	33.7	Bijl et al. (2018b)
DY087, 09PC, 307–312 cm	310	FAD	Dinocyst	<i>Impagidinium aculeatum</i>	34.4	Bijl et al. (2018b)
DY087, 09PC, 307–312 cm	310	FAD	Dinocyst	<i>Impagidinium velorum</i>	33.7	Bijl et al. (2018b)
DY087, 09PC, 307–312 cm	310	FAD	Dinocyst	<i>Impagidinium patulum</i>	33.7	Bijl et al. (2018b)

samples would have an age of ~ 23.7 Ma. Therefore, we conclude that the sediments recovered in core DY087-15PC from 120–234 cm depth have a late Oligocene age (26.4–23.8 Ma), while the sediment horizon from 100–105 cm depth may have an earliest Miocene age (< 23.03 Ma) (Table 2).

4.1.2 DY087-09PC

Diatoms examined from a depth of 220 cm in DY087-09PC conservatively indicate an early Miocene age between 20.8 and 17.4 Ma based on the presence of *Cavitatus miocenicus* (FAD: ~ 24 Ma), *Dactyliosolen* sp. (FAD: ~ 26 Ma), and *Thalassiosira praeфрага* (FAD: 18.6–20.8 Ma; LAD: 17.4–

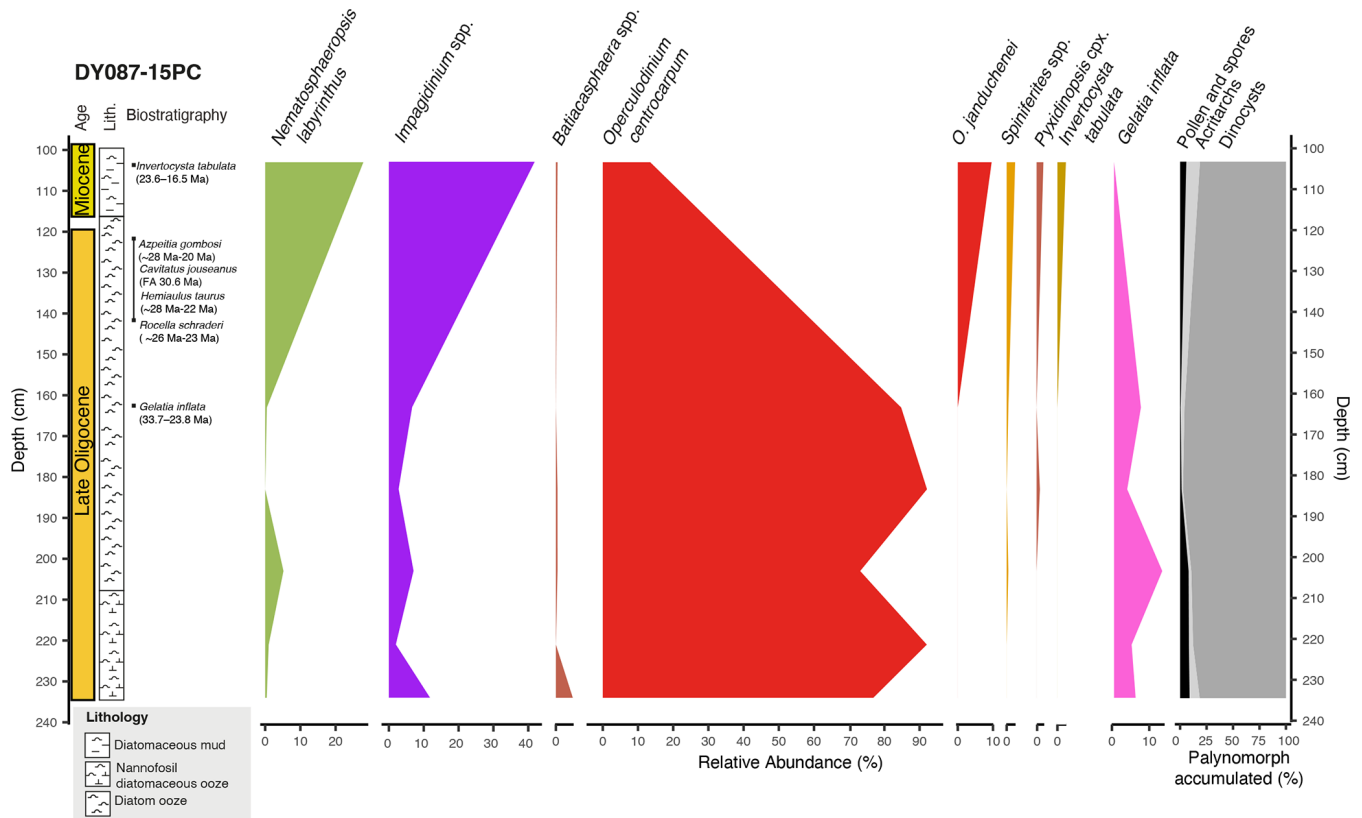


Figure 3. Relative abundances of dinocyst eco-groups (%) and palynomorph relative abundance (acritarchs, dinocysts, and terrestrial palynomorphs) (cumulative %) in core DY087-15PC (Table S3), plotted against core depth, lithology and biostratigraphic age constraints, with bars indicating the time interval. The colours of the dinocyst assemblages correspond to the ecological assemblage groups in the pie charts of Fig. 6.

17.7 Ma) (Table 3), with the younger age limit supported by the absence of *Actinocyclus ingens* (FAD: 15.52–15.83 Ma; Marschalek et al., 2021), *Crucidentacula kanayae* (FAD: 17.9 Ma), and *Denticulopsis maccollumii* (FAD: 16.7 Ma) (see recent compilation of diatom event ages in McKay et al., 2019; Marschalek et al., 2021). The dinocyst assemblage is characterized by the presence of several *Impagidinium* species together with *Operculodinium janduchenei*, which first occurred in the late Eocene and late Oligocene, respectively (Bijl et al., 2018b). The presence of *Invertocysta tabulata* throughout the interval of 63–310 cm indicates a late Oligocene (23.6 Ma) to early Miocene (16.5 Ma) age (Bijl et al., 2018b). Dinocyst assemblages provide no additional age constraints to those provided by diatom biostratigraphy for core DY087-09PC. The sediment sequence recovered in core DY087-09PC most likely represents a short time interval within the age constraints of the diatom ages (Table 3). Because of this, we refer to the age of the studied sediments of core DY087-09PC (interval 63–310 cm) as early Miocene (20.8–17.4 Ma).

4.1.3 ODP Site 696

For this site, we apply the age constraints in López-Quirós et al. (2018) for the Eocene–Oligocene part of the sequence (Cores 59R–53R). The reworked nature of the rhythmically interbedded sandy mudstones with glauconite-bearing sandstone beds of Cores 52R and 51R (548.9 to 529.8 m b.s.f., López-Quirós et al., 2020) hampers an accurate dating of this interval (Table S1). In our palynological analysis we detected the occurrence of dinocyst species *Gelatia inflata* (age range 33.7–23 Ma, Bijl et al., 2018a) in Core 51R-1 (143–145 cm) at 531.23 m b.s.f., indicating an Oligocene age for this core interval. At the top of Core 51R (529 m b.s.f.) there is likely a break in sedimentation (hiatus). The muddy diatomaceous ooze in Core 50R (522–520.6 m b.s.f.) was dated by diatom biostratigraphy both initially onboard during the expedition (Barker et al., 1988) and in more detail post-cruise using Neogene diatom zonations (Gersonde et al., 1990). Gersonde et al. (1990) assigned an early–middle Miocene age (*N. grossepunctata* Zone) to Core 50R based on the first occurrence of the diatom *Denticulopsis maccollumii*, which indicates an age of ≤ 16.7 Ma according to Southern Ocean diatom biostratigraphy (Censarek and Gersonde,

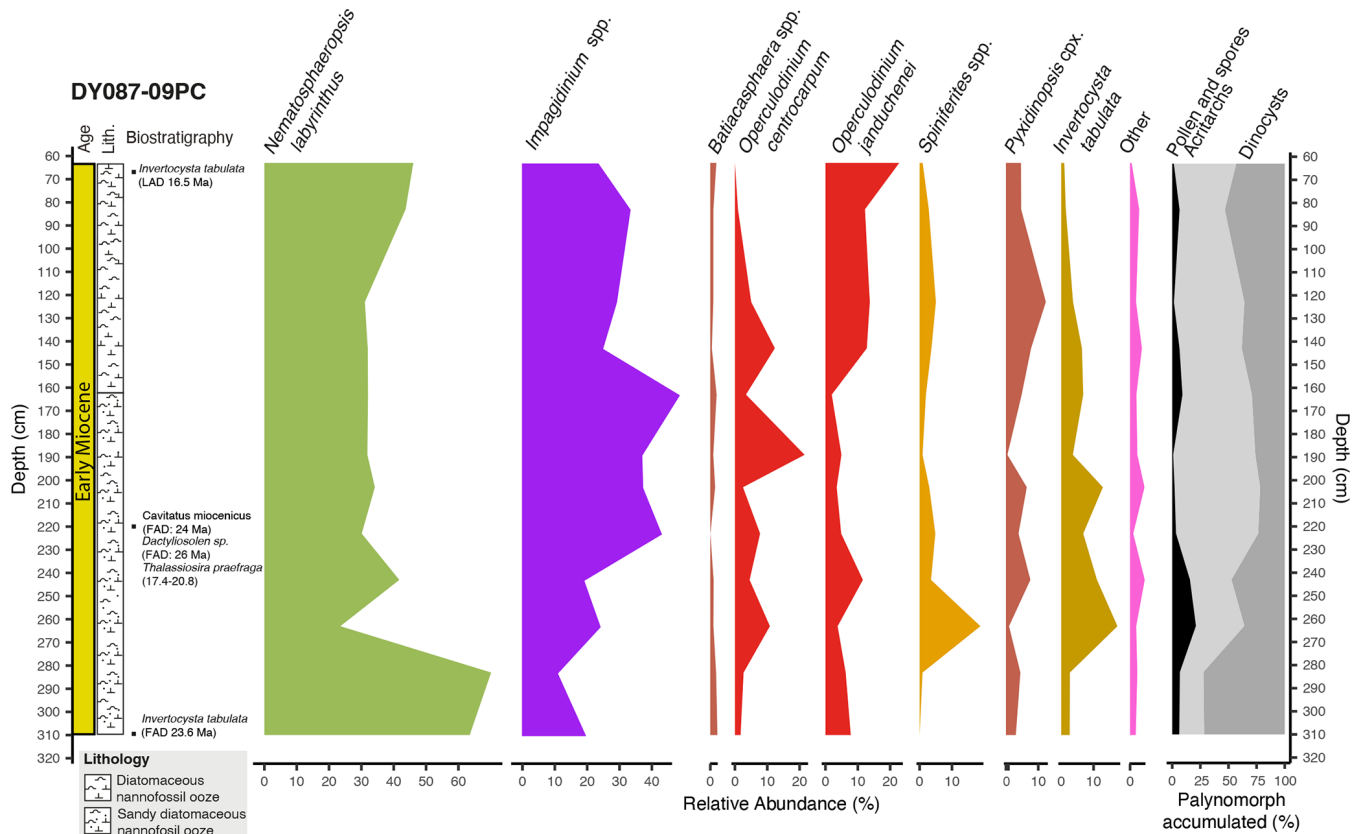


Figure 4. Relative abundances of dinocyst eco-groups (%) and palynomorph relative abundance (pollen and spores, acritarchs, and dinocysts) (cumulative %) in core DY087-09PC (Table S4), plotted against core depth, lithology and biostratigraphic age constraints, with bars indicating the time interval. The colours of the dinocyst assemblages correspond to the ecological assemblage groups in the pie charts of Fig. 6.

2002; McKay et al., 2019; Marschalek et al., 2021). More recently, a thorough review of age-deterministic diatoms (*Denticulopsis maccollumii* and *Actinocyclus ingens*) has further narrowed the age interval of Core 50R to 16.7–16.5 Ma (Table S1; López-Quirós et al., 2018; Hoem et al., 2023).

4.2 Organic-walled dinoflagellate cyst assemblages

4.2.1 DY087-15PC

Dinocyst assemblages in core DY087-15PC (Fig. 3, Table S3) are exclusively dominated by G-cysts, predominantly *Operculodinium centrocarpum* (up to 91 %), with minor contributions from *Gelatia inflata* and rare contributions from *Nematosphaeropsis labyrinthus*. In the uppermost sample analysed from this core (100–105 cm), the palynological assemblage differs significantly from that in the underlying samples by showing a much higher diversity; relatively high abundances of *Nematosphaeropsis labyrinthus* (26.6 %), *Impagidinium velorum* (17.9 %), and *Impagidinium pallidum* (17.0 %); and minor contributions of *Operculodinium centrocarpum* and *Operculodinium janduchenei*. Due to the large age range (23–16.5 Ma) and the fact that it is one single sam-

ple from this uppermost interval, we exclude this single sample from further interpretation (Fig. 6).

4.2.2 DY087-09PC

The dinocyst assemblages in core DY087-09PC consist exclusively of G-cysts (Fig. 4, Table S4) and resemble those of the uppermost single sample (100–105 cm) of core DY087-15PC. The diversity is relatively high (14 species). *Nematosphaeropsis labyrinthus* dominates the assemblages, constituting an abundance of up to 68.9 %, with minor abundances of *Impagidinium pallidum*, *Impagidinium velorum*, *Operculodinium janduchenei*, and *Operculodinium centrocarpum*.

4.2.3 ODP Site 696

We processed eight additional samples between 539 and 520 m b.s.f. from ODP Site 696 (Cores 52R–50R) for palynological investigations to extend the published dinocyst record of Houben et al. (2019) (Cores 63R–53R, Fig. 5, Table S5) into the Miocene. Three samples from 539–531 m b.s.f. (Core 52R and 51R) contain only a few dinocysts. The preserva-

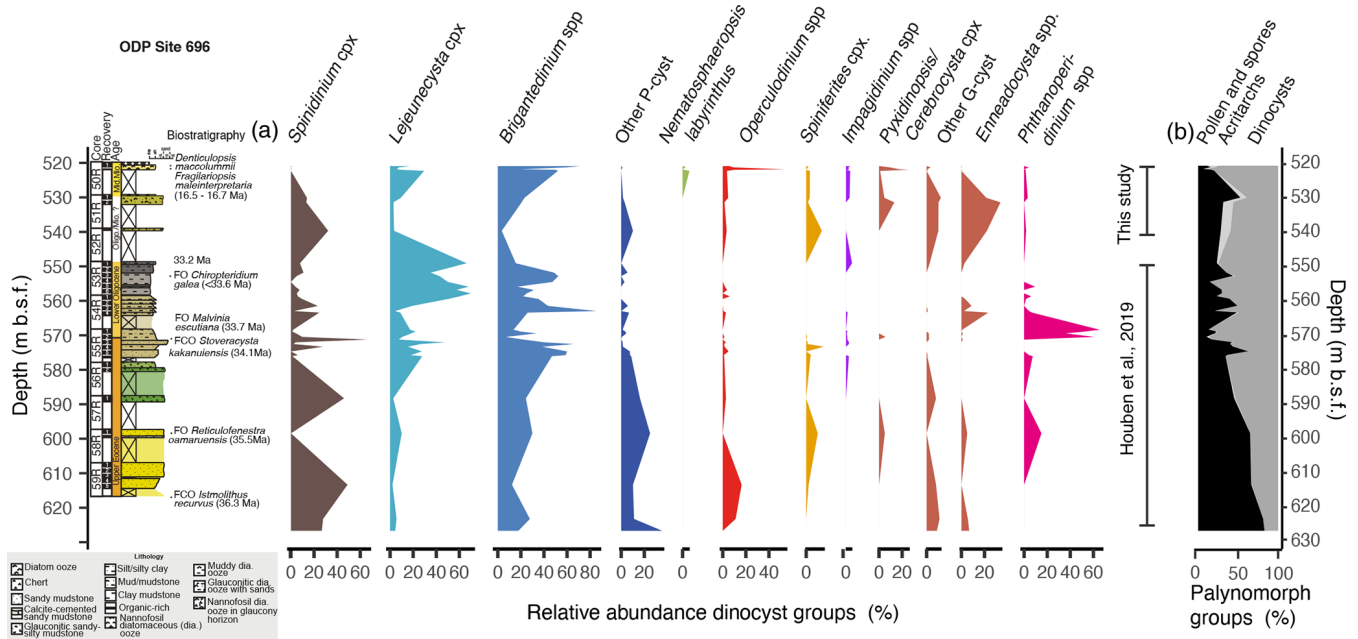


Figure 5. (a) Relative abundance of dinocyst assemblage groups from Houben et al. (2019) and this study (Table S5) plotted vs. depth (m b.s.f.), alongside the lithological log with biostratigraphic age constraints (FO is the first occurrence, while FCO is the first common occurrence) modified after López-Quirós et al. (2019, 2020, 2021), Barker et al. (1988), and Gersonde and Burckle (1990), including new constraints for the uppermost interval (Core 50) from López-Quirós et al. (2018). (b) Relative stacked abundance of pollen and spores (black), acritarchs (light grey), and dinocysts (dark grey) (Houben et al., 2019, this study).

tion of organic matter is poor, and the few dinocysts encountered are mostly typical Eocene species, including *Enneadocysta dictyostila*, *Senegalinum* spp., and *Vozzhennikovia* spp., in addition to the ubiquitous long-ranging *Brigantedinium* spp. and Oligocene species, such as *Gelatia inflata*. Furthermore, since the glauconite-bearing sandstone beds within the rhythmically interbedded sandy mudstones are interpreted to contain reworked grains from underlying (Eocene) intervals (López-Quirós et al., 2020), we take into account that this interval may contain reworked dinocysts. Therefore, we excluded the three samples from Cores 51R–52R from further interpretation in Sect. 5 (Fig. 6). Five samples from 531–520 m b.s.f. depth (Core 50R) with an estimated age of ~16.5 Ma (diatom-based sample, Gersonde et al., 1990; López-Quirós et al., 2018; Hoem et al., 2023) contain abundant, well-preserved, and diverse dinocysts (see Plate S1 for light microscopy photos). All samples are dominated by *Brigantedinium* spp., but in the uppermost samples we note abundant G-cysts, i.e. *Nematosphaeropsis labyrinthus*, *Pyxididnopsis* spp., and *Operculodinium* spp.

4.2.4 IODP Site U1536

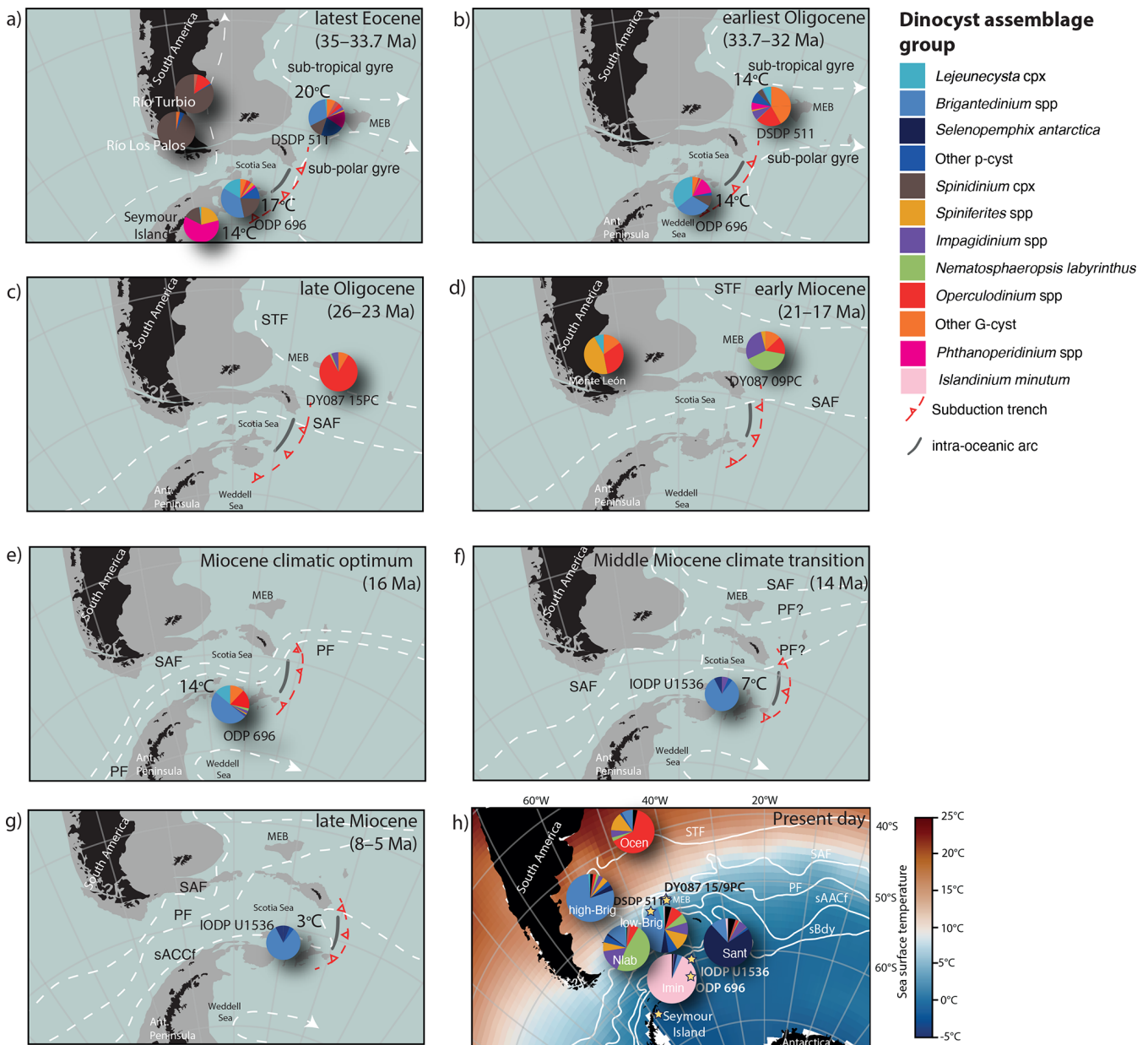
Quantitative analysis of the Miocene sequence recovered at IODP Site U1536 was not possible due to the low number of palynomorphs present in the 20 samples processed. Therefore, we combine our limited observations with the ship-

board analysis conducted by the first author (Weber et al., 2021) and offer only a general overview of the dinocyst assemblages present within the middle and upper Miocene interval (Table S6). The palynomorphs detected in the interval from 638–462 m b.s.f. depth with a middle–late Miocene age predominantly consist of P-cysts: *Brigantedinium* spp., *Selenopemphix antarctica*, and *Lejeunecysta* spp. This indicates that the low abundance of dinocysts does not result from poor preservation in the sediments, as P-cysts are generally more sensitive to degradation under oxic bottom water conditions than autotrophic dinoflagellates producing G-cysts (Zonneveld et al., 2010) but rather that the low abundance of dinocysts is due to dilution by a high rate of accumulation of other sedimentary components. There is an apparent change in the assemblages below 609 m b.s.f. characterized by the disappearance of *Impagidinium* spp. and abundant occurrences of *Lejeunecysta* spp.

5 Discussion

5.1 Latest Eocene–Miocene paleoceanographic changes

We compare our new data of dinocyst assemblages from sites 696, U1536, and DY087-09PC and DY087-15PC with published SW Atlantic Ocean dinocyst records from ODP Site 696 and DSDP Site 511 (Houben et al., 2019); Seymour Is-



land (Douglas et al., 2014); and the South American sites Río Los Palos (Bijl et al., 2021), Río Turbio (Guerstein et al., 2014), and Monte León Formation (Parras et al., 2020), as well as with TEX₈₆-derived SST records (Hoem et al., 2023), to develop a more detailed and comprehensive picture of the paleoceanographic and frontal system changes in the SW Atlantic Ocean (Fig. 6).

5.1.1 The latest Eocene (35–33.7 Ma)

During the latest Eocene (35–33.7 Ma), dinocyst assemblages in the Seymour Island area were dominated by freshwater-tolerant *Phthanoperidinium* spp., which indicates high rates of precipitation and runoff (Douglas et al., 2014) and/or influence of iceberg melting. Temperate SSTs (14–17 °C) just northeast of the Antarctic Peninsula could sustain high precipitation rates in that region with drainage of freshwater into the Weddell Sea. At Site 696, Antarctic endemic taxa, i.e. *Vozzhennikovia* spp. and *Spinidinium* spp., dominate the assemblages together with high abundances of *Deflandrea antarctica*, *Senegalinium* spp. and other P-cysts, suggesting high nutrient concentrations and freshwater input (Houben et al., 2013). Similarly, at DSDP Site 511 in the SW Atlantic Ocean, Antarctic endemic P-cysts were dominant during this time (Houben et al., 2019). This similarity suggests that the subpolar gyre extended relatively far north and brought Antarctic-derived surface waters across both sites in the SW Atlantic Ocean (Fig. 6a). Based on recent investigations of Patagonian shelf dinocyst assemblages, Amenábar et al. (2022) and Guerstein et al. (2023) suggested that abundant Antarctic endemic dinocysts and morphological variability exhibited by the *Turbiosphaera archangelskyi* complex could be linked to a deepening of the Drake Passage promoting cooling and consequent influx of low-salinity water from the shelf. However, we argue that the abundant Antarctic endemic dinocysts at the Patagonian shelf sites Río Turbio (Guerstein et al., 2014; Amenábar et al., 2022) and Río Los Palos (Bijl et al., 2021) indicate that the ocean currents associated with the gyre brought Antarctic-derived surface waters northwards along the eastern South American margin. Our interpretation of a strong, persistent, and large subpolar gyre is consistent with model simulations under closed (England et al., 2017) or shallow gateway configurations (Sauermilch et al., 2021) for the Drake Passage and the Tasmanian Gateway; however, some models already show an effect of high-latitude cooling under shallow open-gateway configurations in the late Eocene (Sijp and England, 2004; Kennedy-Asser et al., 2015, 2019; Toumoulin et al., 2020). Indeed, a breakdown of such a gyre, e.g. one invoked by the opening of Drake Passage, would cause profound cooling of the Antarctic margin (Sauermilch et al., 2021; Hoem et al., 2022). The dinocyst assemblages of the Oligocene should therefore indicate whether the South Atlantic Subpolar Gyre broke down at this time (i.e. in the latest Eocene–earliest Oligocene interval).

5.1.2 The earliest Oligocene (33.7–32 Ma)

In the earliest Oligocene (33.7–32 Ma), the Antarctic endemic taxa were replaced by genera of P-cysts (*Brigantidinium*, *Selenopemphix* and *Lejeunecysta*) at Site 696, probably documenting an increase in upwelling and mixing and higher nutrient availability in the surface waters. Following the EOT (~33.7 Ma), which was marked by declining $p\text{CO}_2$ (Anagnostou et al., 2016), deep-ocean cooling, and the onset of Antarctic glaciation (Coxall et al., 2005), we record high abundances of *Phthanoperidinium* (Fig. 5b). This suggests that significant freshwater input (e.g. Neville et al., 2019) followed the glacial onset due to melting of icebergs in line with the southern Atlantic SST cooling of 3–6 °C (Hoem et al., 2023). The Antarctic endemic and protoperidinioid dinocysts at DSDP Site 511 are abundant in the Eocene sediments (80 %) but decrease to ~27 % of the assemblage in the lower Oligocene when they are replaced by typically offshore cosmopolitan gonyaulacoid taxa (G-cysts) (Houben et al., 2019), suggesting increased oligotrophic conditions. The nutrient gradient between Site 696 and Site 511 increased across the EOT, but the difference in SST at both sites remained stable across the EOT (Tibbett et al., 2022; Hoem et al., 2023), suggesting either intensified deep-ocean circulation (Houben et al., 2019; López-Quirós et al., 2019; 2021) or latitudinal shifts in the region of upwelling rather than a breakdown of gyral circulation. The lack of an increase in SST gradient across the EOT (Hoem et al., 2023) and the continued presence of P-cysts and freshwater-indicative dinocysts at Site 511 suggest that both Site 696 and Site 511 remained under the same oceanographic regime and that Antarctic Ice Sheet formation did not cause an increased SST gradient between these sites. It also implies that deep-water flow through Drake Passage did not change across the EOT, which is in contrast to what modelling results and geologic data suggest (Kennett, 1977; Nicholson and Stow, 2019; Sauermilch et al., 2021). This interpretation is supported by tectonic reconstructions of restricted deep-water throughflow until at least 29 Ma (e.g. Eagles and Jokat, 2014). Furthermore, model-data comparisons show that decreasing atmospheric CO₂, rather than ice sheet forcing or gateway-induced ocean circulation change, played the dominant role in the global cooling across the EOT (Hutchinson et al., 2021). We therefore infer that during the earliest Oligocene the subpolar gyre was still persistent but positioned slightly more to the south than during the Eocene (Fig. 6b).

5.1.3 The late Oligocene (26.4–23 Ma)

The new, short, and low-resolution late Oligocene record from a single site (core DY087-15PC from Maurice Ewing Bank) is exclusively dominated by G-cysts, suggesting low nutrients in the surface waters. However, the absence of any P-cysts may result from oxidation by oxygen-rich bottom waters (Zonneveld et al., 2010). The dinocyst as-

semblage is dominated by *Operculodinium* spp. (> 80%), with a relatively minor presence of *Gelatia inflata* (included within “other G-cysts” in Fig. 7c), *Impagidinium* spp., and *Nematosphaeropsis labyrinthus*, suggesting that the STF was located south of the site. Moreover, dinocysts indicative of sea ice that have been linked to the PF (Prebble et al., 2013) are absent. Ocean models by Sauermilch et al. (2021) suggest that as the Drake Passage deepened below 300 m (given that the Tasmanian Gateway was already deep, i.e. > 1000 m), even a weak proto-ACC penetrating through the deeper Drake Passage would weaken and shrink the subpolar gyre. A weaker subpolar gyre would transport less water northward, thereby causing surface water cooling at the Antarctic continental margin. Tectonic reconstructions of van de Lagemaat et al. (2021), building on earlier work of Eagles and Jokat (2014) and Livermore et al. (2007), suggest that formation of oceanic crust in the western Scotia Sea, which coincided with deepening of Drake Passage and the establishment of the first deep-water connections between isolated ocean basins in the Scotia Sea, happened around 26 Ma. The primary consequence of this deepening of Drake Passage, confirmed by the dinocyst data, is a southward shift in the STF, which may be associated with a weakening of the subpolar gyre because of stronger Drake Passage throughflow. Furthermore, increased late Oligocene Drake Passage throughflow is indicated by sedimentological evidence for enhanced bottom-current vigour and current-induced erosion in South Pacific sediments (Lyle et al., 2007) and by a higher temperature gradient in the Australo-Antarctic Gulf (Hoem et al., 2022). Since the record for this interval is from only a single core site, a better geographical and temporal spread of dinocyst records in the southern Atlantic is needed to confirm this.

5.1.4 The early Miocene (20.8–17.4 Ma)

By the early Miocene (20.8–17.4 Ma), the dominance of *Nematosphaeropsis labyrinthus* at Site DY087-09PC from Maurice Ewing Bank suggests that the STF had migrated northwards. Unfortunately, we do not have any southern Atlantic SST reconstructions for the late Oligocene and early Miocene to confirm this inference. In paleogeographic reconstructions published for this time interval, submerged continental fragments in the Scotia Sea started to move farther apart (Barker, 2001; Pérez et al., 2019; van de Lagemaat et al., 2021), which allowed for more ACC throughflow. We suggest that this stronger water exchange through the Scotia Sea forced the STF to migrate north of Maurice Ewing Bank, as is reflected in the change in the dinocyst assemblages between the upper Oligocene and the lower Miocene sediments.

5.1.5 The Miocene Climatic Optimum (~ 16 Ma)

In the new low-resolution Miocene (~ 16 Ma) dinocyst record from a single site (Site 696), the high abundance of P-cysts suggests that the site was located south of the PF. However, the relatively high SSTs and the common occurrence of the temperate dinocysts *Operculodinium* spp. and *Nematosphaeropsis labyrinthus* and the cosmopolitan species *Spiniferites* spp. suggest that the SAF was likely located further south in the Scotia Sea until at least 16 Ma based on the relatively high abundance (35%) of temperate G-cysts. The Miocene Climatic Optimum (MCO, ~ 17–15 Ma) represents a warm phase when the Antarctic Ice Sheet was reduced in size (Shevenell et al., 2008; Sangiorgi et al., 2018; Foster et al., 2012). The high atmospheric $p\text{CO}_2$ (Sosdian et al., 2020) and intensification and poleward shift in the Southern Hemisphere westerly winds (Toggweiler, 2009) could potentially force frontal systems closer to Antarctica. Alternatively, the tectonic configuration of Drake Passage could have routed these fronts closer to the Antarctic continent than today (Eagles and Jokat, 2014).

5.1.6 Middle Miocene Climate Transition (~ 14 Ma)

The temperate and oligotrophic dinocysts present in the MCO sequence at Site U1536 were replaced by abundant high-nutrient-affiliated *Brigantedinium* spp. and the sea ice indicator *Selenopemphix antarctica* at ~ 14 Ma during the Middle Miocene Climate Transition (MMCT). The major change in surface water environment co-occurred with an average cooling from 14 to ~ 6°C in the TEX_{86} SST record (Hoem et al., 2023), indicating that the SAF had migrated northwards. A similar shift in surface water fauna is recorded at Kerguelen Plateau at 13.8 Ma, when warm-water-affiliated planktonic foraminiferal assemblages were replaced by polar-affiliated assemblages (Verducci et al., 2009; Majewski and Bohaty, 2010), which is attributed to a northward PF migration across Kerguelen Plateau. Furthermore, between ~ 14.5 and 12.0 Ma, neodymium isotope records at Kerguelen Plateau reflect increased inflow of Pacific waters, indicating the establishment of deep eastward oceanic circulation via Drake Passage (Evangelinos et al., 2024). The loss of temperate dinocysts together with decreasing SSTs is consistent with a drop in atmospheric $p\text{CO}_2$ (below 300 ppm; Badger et al., 2013) and coincident with a large, 1.5‰ increase in benthic foraminiferal $\delta^{18}\text{O}$ between ~ 13.9 and 13.8 Ma (Shevenell et al., 2008; Leutert et al., 2020), indicating global cooling and/or increasing ice volume. Frequent erosional unconformities characterizing drill core records from the Ross Sea continental shelf throughout the MMCT (Levy et al., 2016; McKay et al., 2016; Levy et al., 2019; Pérez et al., 2022) indicate rapid seaward Antarctic Ice Sheet expansion. This is interpreted as a larger-than-modern Antarctic Ice Sheet (Holbourn et al., 2005), although novel clumped isotope thermometry suggests that the bulk

of the $\delta^{18}\text{O}$ shift could be attributed to deep-sea cooling (e.g. Hou et al., 2023). At Site U1536, we observe for the first time the occurrence of the sea-ice-affiliated *Selenopemphix antarctica* (albeit in relatively low numbers) at ~ 14 Ma, which suggests expansion of sea ice in the Weddell Sea. The change to present-day-like dinocyst assemblages occurred earlier in the Atlantic sector at Site U1536 than in the Indian sector of the Southern Ocean offshore Wilkes Land (Site U1356), where marine sediments contained abundant G-cysts until at least 11 Ma (Sangiorgi et al., 2018). This is also consistent with findings by Hoem et al. (2023), which show that SSTs in the SW Atlantic Ocean were cooler compared to the southern Pacific and southern Indian oceans. However, unlike Site U1356 offshore Wilkes Land, which recorded the presence of *Islandinium*, this species remained absent in the southern Scotia Sea during this time. Today *Islandinium* is affiliated with cold waters and fresh (melt)water input and dominates the dinocyst assemblages in sediments from the southern Scotia Sea (Thöle et al., 2023), where freshwater input through melting icebergs is high (Stuart and Long, 2011). The absence of *Islandinium* might result from reduced iceberg discharge or indicate that iceberg drift followed a different path or that most of these icebergs melted at a different location.

5.1.7 The late Miocene (8–5 Ma)

Following the MMCT, seismic analysis around Site U1536 (Pérez et al., 2021) indicates reorganization of the regional sedimentary stacking pattern leading to the formation of Reflector-c, which coincides with a period of non-deposition or erosion in our record between 14.2 and 8.4 Ma. This time interval also coincides with increases in benthic foraminiferal $\delta^{18}\text{O}$ values, indicating deep-ocean cooling and an ice volume increase. Furthermore, the late Miocene global eustatic sea level is estimated to have been relatively low (Adams et al., 1977; Miller et al., 2005; Rohling et al., 2022). Astronomical configurations of low obliquity and eccentricity during this time are believed to have favoured the onset of perennial sea ice cover (Levy et al., 2019) and ice sheet expansion in West Antarctica (Anderson et al., 2011). The complete disappearance of *Impagidinium* and more common occurrence of *S. antarctica* in the late Miocene (8–5 Ma) dinocyst record at Site U1536 and colder average SSTs (3°C) confirm a cooling of surface waters and stronger sea ice influence. This cooling must have further weakened the Weddell Gyre. With reconstructions of deep-water flow through the northern end of the eastern Scotia Sea by ~ 10 Ma (Eagles and Jokat, 2014) and full Drake Passage opening by 6 Ma (Barker et al., 2007), we assume that the ACC fronts migrated northwards (e.g. Maldonado et al., 2006; Pérez et al., 2019) towards modern configurations and that the ACC strengthened in the late Miocene, consistent with recent findings (Evangelinos et al., 2024).

6 Conclusions

Based on our comprehensive analysis of the SW Atlantic Ocean dinocyst assemblages, we infer a persistent circulation of the subpolar gyre throughout the Eocene–Oligocene transition (EOT) consistent with recent SST reconstructions (Fig. 6). The disappearance of Antarctic endemic and typical cold-water-indicative dinocysts northeast of Drake Passage by the mid-Oligocene (between 32 and 26 Ma) suggests a breakdown of the dominant gyral circulation and strengthening of frontal systems, separating the warm subtropics from the polar Antarctic margin. A northward migration of the STF past Maurice Ewing Bank occurred in the early Miocene. The oligotrophic, warmer-water-indicative dinocysts present during the Miocene Climatic Optimum (16 Ma) were replaced by protoperidinioid and heterotrophic dinocysts after the Middle Miocene Climate Transition (14 Ma), indicating the presence of high-nutrient, cold, sea-ice-influenced surface water conditions in the SW Atlantic Ocean at 14 Ma. In parallel, TEX_{86} SSTs dropped from 14 to $7\text{--}5^\circ\text{C}$. The appearance of more common sea-ice-affiliated dinocysts and the complete loss of typical sub-tropical, oligotrophic dinocyst assemblages by the late Miocene (8–5 Ma) confirm the onset of modern-like conditions with northward migration of frontal systems and expansion of sea ice. Although some intervals are covered by just one or a few locations and many gaps in the sedimentary archives hamper a complete record of oceanographic change in the late Cenozoic SW Atlantic Ocean, our compilation shows, for the first time, the stepwise breakdown of the large South Atlantic Subpolar Gyre into the modern-like oceanographic regime with a strong Antarctic Circumpolar Current, frontal systems, and temperature gradients across a narrow band of latitudes.

Data availability. Microscope slides are stored in the collection of the Utrecht University Marine Palynology and Paleoceanography group (017.560, 017.556, 017.555, 017.554). The supplementary dinocyst data (Tables S3–S6) are available in the Supplement and will also be available from the Zenodo data repository (Hoem et al., 2024, <https://doi.org/10.5281/zenodo.14262307>).

Supplement. Tables S1–S2, Plate S1, and larger data tables (Tables S3–S6) are included in the Supplement (Table S3: DY087-15PC dinocyst dataset; Table S4: DY087-09PC dinocyst dataset; Table S5: ODP Site 696 dinocyst dataset; Table S6: IODP Site U1536 dinocyst dataset). The supplement related to this article is available online at: <https://doi.org/10.5194/jm-43-497-2024-supplement>.

Author contributions. PKB and FS designed the research. SMB provided the samples, age model, and sedimentary information for the DY087 cores. KvdB quantified the palynomorphs in the DY087

palynological slides. FSH controlled the dinocyst counts. SMB, CDH, RDL, and TEvP provided samples, site and depositional information, and diatom age constraints for DY087 piston cores. ALQ provided depositional information and age constraints for ODP Site 696. FH processed and analysed Site 696 samples for palynology. FSH, PKB, and FS interpreted the palynological results. SHAvdL advised on the Drake Passage tectonic evolution. All authors provided input for the writing of the paper.

Competing interests. At least one of the (co-)authors is a member of the editorial board of *Journal of Micropalaeontology*. The peer-review process was guided by an independent editor, and the authors also have no other competing interests to declare.

Disclaimer. Publisher’s note: Copernicus Publications remains neutral with regard to jurisdictional claims made in the text, published maps, institutional affiliations, or any other geographical representation in this paper. While Copernicus Publications makes every effort to include appropriate place names, the final responsibility lies with the authors.

Special issue statement. This article is part of the special issue “Advances in Antarctic chronology, paleoenvironment, and paleoclimate using microfossils: Results from recent coring campaigns”. It is not associated with a conference.

Acknowledgements. We thank the International Ocean Discovery Program (IODP) and their precursor drilling programs for collecting, storing, and providing the sediment materials used for our analysis. We thank the scientists, crew, and technicians of IODP Expedition 382 “Iceberg Alley” and RRS *Discovery* cruise DY087. Cruise DY087 was supported by NERC grant nos. NE/M021254/1 and NE/M021270/1, and sample material from the DY087 cores was provided by the British Ocean Sediment Core Research Facility (BOSCORF). We additionally thank BOSCORF for the use of their laboratory space and generous staff assistance with core processing and sampling. We thank Natasja Welters and Giovanni Dammers for the processing of palynological samples. Adrián López-Quirós acknowledges funding provided by the Spanish Ministry of Science and Innovation, grant numbers CTM2014-60451-C2-1/2-P and CTM2017-89711-C2-1/2-P (co-funded by the European Union through FEDER funds) and for Research Contract FJC2021-047046-I (MCIN/AEI/10.13039/501100011033 and NextGenerationEU/PRTR). Frida S. Hoem also acknowledges her current funding at the University of Bergen (as of 2024) from the European Union’s Horizon 2020 Research And Innovation Programme, under Marie Skłodowska-Curie grant agreement no. 101034309 “Shaping European Research Leaders for Marine Sustainability (SEAS)”. Tim E. van Peer was also supported by NERC grant no. NE/M021254/1. We highly appreciate the anonymous reviewer, Marcelo A. De Lira Mota, and the topic editor Denise K. Kulhanek for their thorough and constructive feedback, suggestions, and discussions that helped improve the manuscript.

Financial support. This research has been supported by the Dutch Research Council (Nederlandse Organisatie voor Wetenschappelijk Onderzoek, NWO) polar programme (grant no. ALW.2016.001), and the European Research Council H2020 programme (grant no. OceaNice 802835).

Review statement. This paper was edited by Denise K. Kulhanek and reviewed by Marcelo De Lira Mota and one anonymous referee.

References

- Adams, C., Benson, R. H., Kidd, R., Ryan, W., and Wright, R.: The Messinian salinity crisis and evidence of late Miocene eustatic changes in the world ocean, *Nature*, 269, 383–386, 1977.
- Amenábar, C. R., Guerin, G. R., Alperin, M. I., Palma, E. D., Casadío, S., Belgaburo, A., and Rodríguez Raising, M.: Eocene palaeoenvironments and palaeoceanography of areas adjacent to the Drake Passage: insights from dinoflagellate cyst analysis, *Palaeontology*, 65, e12601, <https://doi.org/10.1111/pala.12601>, 2022.
- Anagnostou, E., John, E. H., Edgar, K. M., Foster, G. L., Ridgwell, A., Inglis, G. N., Pancost, R. D., Lunt, D. J., and Pearson, P. N.: Changing atmospheric CO₂ concentration was the primary driver of early Cenozoic climate, *Nature*, 533, 380–384, 2016.
- Anderson, J. B., Warny, S., Askin, R. A., Wellner, J. S., Bohaty, S. M., Kirshner, A. E., Livsey, D. N., Simms, A. R., Smith, T. R., and Ehrmann, W.: Progressive Cenozoic cooling and the demise of Antarctica’s last refugium, *P. Natl. Acad. Sci. USA*, 108, 11356–11360, 2011.
- Badger, M. P., Lear, C. H., Pancost, R. D., Foster, G. L., Bailey, T. R., Leng, M. J., and Abels, H. A.: CO₂ drawdown following the middle Miocene expansion of the Antarctic Ice Sheet, *Paleoceanography*, 28, 42–53, 2013.
- Barke, J., Abels, H. A., Sangiorgi, F., Greenwood, D. R., Sweet, A. R., Donders, T., Reichert, G.-J., Lotter, A. F., and Brinkhuis, H.: Orbitally forced *Azolla* blooms and Middle Eocene Arctic hydrology: Clues from palynology, *Geology*, 39, 427–430, 2011.
- Barker, P. F., Kennett, J. P., O’Connell, S., Berkowitz, S., Bryant, W. R., Burckle, L. H., Egeberg, P. K., Futterer, D. K., Gersonde, R. E., and Golovchenko, X.: Proceedings of the Ocean Drilling Program, Initial Reports, Vol. 113, Weddell Sea, Antarctica. Covering Leg 113 of the cruises of the drilling vessel JOIDES Resolution, Valparaiso, Chile, to East Cove, Falkland Islands, Sites 689–697, 25 December 1986–11 March 1987, <https://doi.org/10.2973/odp.proc.ir.113.1988>, 1988.
- Barker, P. and Burrell, J.: The opening of Drake passage, *Mar. Geol.*, 25, 15–34, 1977.
- Barker, P. F.: Scotia Sea regional tectonic evolution: implications for mantle flow and palaeocirculation, *Earth-Sci. Rev.*, 55, 1–39, 2001.
- Barker, P. F., Filippelli, G. M., Florindo, F., Martin, E. E., and Scher, H. D.: Onset and role of the Antarctic Circumpolar Current, *Deep-Sea Res. Pt. II*, 54, 2388–2398, 2007.
- Bijl, P. K., Pross, J., Warnaar, J., Stickley, C. E., Huber, M., Guerin, R., Houben, A. J., Sluijs, A., Visscher, H., and Brinkhuis, H.: Environmental forcings of Paleogene South-

- ern Ocean dinoflagellate biogeography, *Paleoceanography*, 26, PA1202, <https://doi.org/10.1029/2009PA001905>, 2011.
- Bijl, P. K., Bendle, J. A., Bohaty, S. M., Pross, J., Schouten, S., Tauxe, L., Stickley, C. E., McKay, R. M., Röhl, U., and Olney, M.: Eocene cooling linked to early flow across the Tasmanian Gateway, *P. Natl. Acad. Sci. USA*, 110, 9645–9650, 2013.
- Bijl, P. K., Houben, A. J. P., Hartman, J. D., Pross, J., Salabarnada, A., Escutia, C., and Sangiorgi, F.: Paleoclimatology and ice sheet variability offshore Wilkes Land, Antarctica – Part 2: Insights from Oligocene–Miocene dinoflagellate cyst assemblages, *Clim. Past*, 14, 1015–1033, <https://doi.org/10.5194/cp-14-1015-2018>, 2018a.
- Bijl, P. K., Houben, A. J. P., Bruls, A., Pross, J., and Sangiorgi, F.: Stratigraphic calibration of Oligocene–Miocene organic-walled dinoflagellate cysts from offshore Wilkes Land, East Antarctica, and a zonation proposal, *J. Micropalaeontol.*, 37, 105–138, <https://doi.org/10.5194/jm-37-105-2018>, 2018b.
- Bijl, P., Guerin, R., Sanmiguel Jaimes, E., Sluijs, A., Casadio, S. A., Valencia, V., Amenábar, C., and Encinas, A.: Campanian–Eocene dinoflagellate cyst biostratigraphy in the Southern Andean foreland basin: Implications for Drake Passage throughflow, *Andean Geol.*, 48, 185–218, <https://doi.org/10.5027/andgeoV48n2-3339>, 2021.
- Bijl, P. K.: DINOSTRAT: a global database of the stratigraphic and paleolatitudinal distribution of Mesozoic–Cenozoic organic-walled dinoflagellate cysts, *Earth Syst. Sci. Data*, 14, 579–617, <https://doi.org/10.5194/essd-14-579-2022>, 2022.
- Brinkhuis, H.: Late Eocene to Early Oligocene dinoflagellate cysts from the Priabonian type-area (Northeast Italy): biostratigraphy and paleoenvironmental interpretation, *Palaeogeogr. Palaeoclimatol.*, 107, 121–163, [https://doi.org/10.1016/0031-0182\(94\)90168-6](https://doi.org/10.1016/0031-0182(94)90168-6), 1994.
- Censarek, B. and Gersonde, R.: Miocene diatom biostratigraphy at ODP Sites 689, 690, 1088, 1092 (Atlantic sector of the Southern Ocean), *Mar. Micropaleontol.*, 45, 309–356, 2002.
- Ciesielski, P. F. and Wise Jr, S. W.: Geologic history of the Maurice Ewing Bank of the Falkland Plateau (southwest Atlantic sector of the Southern Ocean) based on piston and drill cores, *Mar. Geol.*, 25, 175–207, 1977.
- Ciesielski, P. F., Ledbetter, M. T., and Ellwood, B. B.: The development of Antarctic glaciation and the Neogene paleoenvironment of the Maurice Ewing Bank, *Mar. Geol.*, 46, 1–51, 1982.
- Clowes, C. D., Hannah, M. J., Wilson, G. J., and Wrenn, J. H.: Marine palynostratigraphy and new species from the Cape Roberts drill-holes, Victoria land basin, Antarctica, *Mar. Micropaleontol.*, 126, 65–84, <https://doi.org/10.1016/j.marmicro.2016.06.003>, 2016.
- Cody, R. D., Levy, R. H., Harwood, D. M., and Sadler, P. M.: Thinking outside the zone: High-resolution quantitative diatom biochronology for the Antarctic Neogene, *Palaeogeogr. Palaeoclimatol.*, 260, 92–121, <https://doi.org/10.1016/j.palaeo.2007.08.020>, 2008.
- Coxall, H. K., Wilson, P. A., Pälike, H., Lear, C. H., and Backman, J.: Rapid stepwise onset of Antarctic glaciation and deeper calcite compensation in the Pacific Ocean, *Nature*, 433, 53–57, 2005.
- Crouch, E., Mildenhall, D., and Neil, H.: Distribution of organic-walled marine and terrestrial palynomorphs in surface sediments, offshore eastern New Zealand, *Mar. Geol.*, 270, 235–256, <https://doi.org/10.1016/j.jears.2019.102961>, 2019.
- Dale, B.: Dinoflagellate cyst ecology: modeling and geological applications, *Palynology: principles and applications*, in: *Palynology: principles and applications*, Vol. 3, 1249–1275, American Association of Stratigraphic Palynologists Foundation, 1996.
- De Schepper, S., Fischer, E. I., Groeneveld, J., Head, M. J., and Matthiessen, J.: Deciphering the palaeoecology of Late Pliocene and Early Pleistocene dinoflagellate cysts, *Palaeogeogr. Palaeoclimatol.*, 309, 17–32, <https://doi.org/10.1016/j.palaeo.2011.04.020>, 2011.
- Douglas, P. M., Affek, H. P., Ivany, L. C., Houben, A. J., Sijp, W. P., Sluijs, A., Schouten, S., and Pagani, M.: Pronounced zonal heterogeneity in Eocene southern high-latitude sea surface temperatures, *P. Natl. Acad. Sci. USA*, 111, 6582–6587, 2014.
- Duncan, B., McKay, R., Levy, R., Naish, T., Prebble, J., Sangiorgi, F., Krishnan, S., Hoem, F., Clowes, C., and Dunkley Jones, T.: Climatic and tectonic drivers of late Oligocene Antarctic ice volume, *Nat. Geosci.*, 15, 819–825, 2022.
- England, M. H., Hutchinson, D. K., Santoso, A., and Sijp, W. P.: Ice–atmosphere feedbacks dominate the response of the climate system to Drake Passage closure, *J. Clim.*, 30, 5775–5790, <https://doi.org/10.1175/JCLI-D-15-0554.1>, 2017.
- Esper, O. and Zonneveld, K. A.: Distribution of organic-walled dinoflagellate cysts in surface sediments of the Southern Ocean (eastern Atlantic sector) between the Subtropical Front and the Weddell Gyre, *Mar. Micropaleontol.*, 46, 177–208, 2002.
- Esper, O. and Zonneveld, K. A.: The potential of organic-walled dinoflagellate cysts for the reconstruction of past sea-surface conditions in the Southern Ocean, *Mar. Micropaleontol.*, 65, 185–212, 2007.
- Eagles, G. and Jokat, W.: Tectonic reconstructions for paleobathymetry in Drake Passage, *Tectonophysics*, 611, 28–50, 2014.
- Evangelinos, D., Escutia, C., Etourneau, J., Hoem, F., Bijl, P., Boterblom, W., van de Flierdt, T., Valero, L., Flores, J.-A., Rodríguez-Tovar, F. J., Jiménez-Espejo, F. J., Salabarnada, A., and López-Quirós, A.: Late Oligocene–Miocene proto-Antarctic Circumpolar Current dynamics off the Wilkes Land margin, East Antarctica, *Glob. Planet. Change*, 191, 103221, <https://doi.org/10.1016/j.gloplacha.2020.103221>, 2020.
- Evangelinos, D., Etourneau, J., van de Flierdt, T., Crosta, X., Jandiel, C., Flores, J.-A., Harwood, D. M., Valero, L., Ducassou, E., and Sauermilch, I.: Late Miocene onset of the modern Antarctic Circumpolar Current, *Nat. Geosci.*, 17, 165–170, <https://doi.org/10.1038/s41561-023-01356-3>, 2024.
- Foster, G. L., Lear, C. H., and Rae, J. W.: The evolution of $p\text{CO}_2$, ice volume and climate during the middle Miocene, *Earth Planet. Sc. Lett.*, 341, 243–254, 2012.
- Frieling, J. and Sluijs, A.: Towards quantitative environmental reconstructions from ancient non-analogue microfossil assemblages: Ecological preferences of Paleocene – Eocene dinoflagellates, *Earth-Sci. Rev.*, 185, 956–973, <https://doi.org/10.1016/j.jears.2018.08.014>, 2018.
- Garabato, A. C. N., Heywood, K. J., and Stevens, D. P.: Modification and pathways of Southern Ocean deep waters in the Scotia Sea, *Deep-Sea Res. Pt. I*, 49, 681–705, 2002.
- GEBCO: The General Bathymetric Chart of the Oceans, GEBCO, <https://www.gebco.net> (last access: 18 November 2023), 2023.

- Gersonde, R., Abelmann, A., Burckle, L. H., Hamilton, N., Lazarus, D., McCartney, K., O'Brien, P., Spieß, V., and Wise Jr., S. W.: Biostratigraphic synthesis of Neogene siliceous microfossils from the Antarctic ocean, ODP Leg 113 (Weddell Sea), in: *Proceedings of the Ocean Drilling Program, Scientific Results*, Vol. 113, edited by: Barker, P. F., Kennett, J. P., O'Connell, S., Berkowitz, S. P., Bryant, W. R., Burckle, L. H., Egeberg, P. K., Fuetterer, D. K., Gersonde, R. E., Golovchenko, X., Hamilton, N., Lawver, L. A., Lazarus, D. B., Lonsdale, M. J., Mohr, B. A., Nagao, T., Pereira, C. P. G., Pudsey, C. J., Robert, C. M., Schandl, E. S., Spieß, V., Stott, L. D., Thomas, E., Thompson, K. F. M., Wise Jr., S. W., and Stewart, N. J., College Station, TX (Ocean Drilling Program), 915–936, <https://doi.org/10.2973/odp.proc.sr.113.209.1990>, 1990.
- Guerstein, G. R., Guler, M. V., Williams, G. L., Fensome, R. A., and Chiesa, J. O.: Middle Palaeogene dinoflagellate cysts from Tierra del Fuego, Argentina: biostratigraphy and palaeoenvironments, *J. Micropalaeontol.*, 27, 75–94, <https://doi.org/10.1144/jm.27.1.75>, 2008.
- Guerstein, G. R., Guler, M. V., Brinkhuis, H., and Warnaar, J.: Mid Cenozoic palaeoclimatic and palaeoceanographic trends in the southwest Atlantic Basins, a dinoflagellate view. The paleontology of Gran Barranca: Evolution and environmental change through the middle Cenozoic of Patagonia, Cambridge University Press, 398–409, 2010.
- Guerstein, G. R., Estebenet, M. S. G., Alperín, M. I., Casadío, S. A., and Archangelsky, S.: Correlation and palaeoenvironments of middle Paleogene marine beds based on dinoflagellate cysts in southwestern Patagonia, Argentina, *J. South Am. Earth Sci.*, 52, 166–178, 2014.
- Guerstein, G. R., Amenábar, C. R., Fensome, R. A., Daners, G., and Palma, E. D.: *Turbiosphaera archangelskyi* sp. nov. and a morphological complex from the late Middle to Late Eocene of southern high latitudes: Biostratigraphic, palaeoenvironmental and palaeoceanographic implications, *Rev. Palaeobot. Palynol.*, 319, 104991, <https://doi.org/10.1016/j.revpalbo.2023.104991>, 2023.
- Hannah, M. J.: The palynology of ODP site 1165, Prydz Bay, East Antarctica: a record of Miocene glacial advance and retreat, *Palaeogeogr. Palaeoclimatol.*, 231, 120–133, <https://doi.org/10.1016/j.palaeo.2005.07.029>, 2006.
- Harwood, D. M. and Maruyama, T.: Middle Eocene to Pleistocene diatom biostratigraphy of Southern Ocean sediments from the Kerguelen Plateau, Leg 120, in: *Proceedings of the Ocean Drilling Program, Scientific Results*, Vol. 120, edited by: Wise Jr., S. W., Schlich, R., Palmer-Julson, A. A., Aubry, M.-P., Berggren, W. A., Bitschene, P. R., Blackburn, N. A., Breza, J. R., Coffin, M. F., Harwood, D. M., Heider, F., Holmes, M. A., Howard, W. R., Inokuchi, H., Kelts, K., Lazarus, D. B., Mackensen, A., Maruyama, T., Munschy, M., Pratson, E. L., Quilty, P. G., Rack, F. R., Salters, V. J. M., Sevigny, J. H., Storey, M., Takemura, A., Watkins, D. K., Whitechurch, H., Zachos, J., and Barbu, E. M., College Station, TX (Ocean Drilling Program), 683–733, <https://doi.org/10.2973/odp.proc.sr.120.160.1992>, 1992.
- Harland, R. and Pudsey, C. J.: Dinoflagellate cysts from sediment traps deployed in the Bellingshausen, Weddell and Scotia seas, Antarctica, *Mar. Micropalaeontol.*, 37, 77–99, 1999.
- Hartman, J. D., Sangiorgi, F., Salabarnada, A., Peterse, F., Houben, A. J. P., Schouten, S., Brinkhuis, H., Escutia, C., and Bijl, P. K.: Paleooceanography and ice sheet variability offshore Wilkes Land, Antarctica – Part 3: Insights from Oligocene–Miocene TEX86-based sea surface temperature reconstructions, *Clim. Past*, 14, 1275–1297, <https://doi.org/10.5194/cp-14-1275-2018>, 2018.
- Head, M. J., Harland, R., and Matthiessen, J.: Cold marine indicators of the late Quaternary: the new dinoflagellate cyst genus *Islandinium* and related morphotypes, *J. Quaternary Sci.*, 16, 621–636, 2001.
- Herbert, T. D., Lawrence, K. T., Tzanova, A., Peterson, L. C., Caballero-Gill, R., and Kelly, C. S.: Late Miocene global cooling and the rise of modern ecosystems, *Nat. Geosci.*, 9, 843–847, 2016.
- Herold, N., Huber, M., Müller, R., and Seton, M.: Modeling the Miocene climatic optimum: Ocean circulation, *Paleoceanography*, 27, PA1209, <https://doi.org/10.1029/2010PA002041>, 2012.
- Hoem, F. S., Valero, L., Evangelinos, D., Escutia, C., Duncan, B., McKay, R. M., Brinkhuis, H., Sangiorgi, F., and Bijl, P. K.: Temperate Oligocene surface ocean conditions offshore of Cape Adare, Ross Sea, Antarctica, *Clim. Past*, 17, 1423–1442, <https://doi.org/10.5194/cp-17-1423-2021>, 2021a.
- Hoem, F. S., Sauermilch, I., Hou, S., Brinkhuis, H., Sangiorgi, F., and Bijl, P. K.: Late Eocene–early Miocene evolution of the southern Australian subtropical front: a marine palynological approach, *J. Micropalaeontol.*, 40, 175–193, <https://doi.org/10.5194/jm-40-175-2021>, 2021b.
- Hoem, F. S., Sauermilch, I., Aleksinski, A. K., Huber, M., Peterse, F., Sangiorgi, F., and Bijl, P. K.: Strength and variability of the Oligocene Southern Ocean surface temperature gradient, *Commun. Earth Environ.*, 3, 322, <https://doi.org/10.1038/s43247-022-00666-5>, 2022.
- Hoem, F. S., López-Quirós, A., van de Lagemaat, S., Etourneau, J., Sicre, M.-A., Escutia, C., Brinkhuis, H., Peterse, F., Sangiorgi, F., and Bijl, P. K.: Late Cenozoic sea-surface-temperature evolution of the South Atlantic Ocean, *Clim. Past*, 19, 1931–1949, <https://doi.org/10.5194/cp-19-1931-2023>, 2023.
- Hoem, F. S., van den Broek, K., López-Quirós, A., van de Lagemaat, S., Bohaty, S. M., Hillenbrand, C. D., Larter, R. D., Van Peer, T. E., Brinkhuis, H., Sangiorgi, F., and Bijl, P. K.: Stepwise Oligocene–Miocene breakdown of subpolar gyres and strengthening of the Antarctic Circumpolar Current (data sets), *Zenodo* [data set], <https://doi.org/10.5281/zenodo.14262307>, 2024.
- Holbourn, A., Kuhnt, W., Schulz, M., and Erlenkeuser, H.: Impacts of orbital forcing and atmospheric carbon dioxide on Miocene ice-sheet expansion, *Nature*, 438, 483–487, 2005.
- Hou, S., Lamprou, F., Hoem, F. S., Hadju, M. R. N., Sangiorgi, F., Peterse, F., and Bijl, P. K.: Lipid-biomarker-based sea surface temperature record offshore Tasmania over the last 23 million years, *Clim. Past*, 19, 787–802, <https://doi.org/10.5194/cp-19-787-2023>, 2023.
- Hou, S., Stap, L. B., Paul, R., Nelissen, M., Hoem, F. S., Ziegler, M., Sluijs, A., Sangiorgi, F., and Bijl, P. K.: Reconciling Southern Ocean fronts equatorward migration with minor Antarctic ice volume change during Miocene cooling, *Nat. Commun.*, 14, 7230, <https://doi.org/10.1038/s41467-023-43106-4>, 2023.
- Houben, A. J., Bijl, P. K., Pross, J., Bohaty, S. M., Passchier, S., Stickley, C. E., Röhl, U., Sugisaki, S., Tauxe, L., and van de

- Fliedert, T.: Reorganization of Southern Ocean plankton ecosystem at the onset of Antarctic glaciation, *Science*, 340, 341–344, 2013.
- Houben, A. J., Bijl, P. K., Sluijs, A., Schouten, S., and Brinkhuis, H.: Late Eocene Southern Ocean cooling and invigoration of circulation preconditioned Antarctica for full-scale glaciation, *Geochem. Geophys. Geosy.*, 20, 2214–2234, <https://doi.org/10.1029/2019GC008182>, 2019.
- Hou, S., Stap, L., Paul, R., Nelissen, M., Hoem, F., Ziegler, M., Sluijs, A., Sangiorgi, F., and Bijl, P.: Reconciling equatorward migration of Southern Ocean fronts with minor ice volume change during Miocene cooling, *Nat. Commun.*, 14, 7230, <https://doi.org/10.1038/s41467-023-43106-4>, 2023.
- Huber, M., Brinkhuis, H., Stickley, C. E., Döös, K., Sluijs, A., Warnaar, J., Schellenberg, S. A., and Williams, G. L.: Eocene circulation of the Southern Ocean: Was Antarctica kept warm by subtropical waters?, *Paleoceanography*, 19, PA4026, <https://doi.org/10.1029/2004PA001014>, 2004.
- Hutchinson, D. K., Coxall, H. K., Lunt, D. J., Steinthorsdottir, M., de Boer, A. M., Baatsen, M., von der Heydt, A., Huber, M., Kennedy-Asser, A. T., Kunzmann, L., Ladant, J.-B., Lear, C. H., Moraweck, K., Pearson, P. N., Piga, E., Pound, M. J., Salzmann, U., Scher, H. D., Sijp, W. P., Śliwińska, K. K., Wilson, P. A., and Zhang, Z.: The Eocene–Oligocene transition: a review of marine and terrestrial proxy data, models and model–data comparisons, *Clim. Past*, 17, 269–315, <https://doi.org/10.5194/cp-17-269-2021>, 2021.
- Kennedy, A. T., Farnsworth, A., Lunt, D., Lear, C. H., and Markwick, P.: Atmospheric and oceanic impacts of Antarctic glaciation across the Eocene–Oligocene transition, *Philos. T. R. Soc. A*, 373, 20140419, <https://doi.org/10.1098/rsta.2014.0419>, 2015.
- Kennedy-Asser, A., Lunt, D. J., Farnsworth, A., and Valdes, P.: Assessing mechanisms and uncertainty in modeled climatic change at the Eocene–Oligocene transition, *Paleoceanogr. Paleocl.*, 34, 16–34, 2019.
- Kennett, J. P.: Cenozoic evolution of Antarctic glaciation, the circum-Antarctic Ocean, and their impact on global paleoceanography, *J. Geophys. Res.*, 82, 3843–3860, 1977.
- Lagabriele, Y., Goddérís, Y., Donnadieu, Y., Malavieille, J., and Suarez, M.: The tectonic history of Drake Passage and its possible impacts on global climate, *Earth Planet. Sc. Lett.*, 279, 197–211, 2009.
- Leutert, T. J., Auderset, A., Martínez-García, A., Modestou, S., and Meckler, A. N.: Coupled Southern Ocean cooling and Antarctic ice sheet expansion during the middle Miocene, *Nat. Geosci.*, 13, 634–639, 2020.
- Levy, R., Harwood, D., Florindo, F., Sangiorgi, F., Tripathi, R., Von Eynatten, H., Gasson, E., Kuhn, G., Tripathi, A., and DeConto, R.: Antarctic ice sheet sensitivity to atmospheric CO₂ variations in the early to mid-Miocene, *P. Natl. Acad. Sci. USA*, 113, 3453–3458, 2016.
- Levy, R. H., Meyers, S. R., Naish, T. R., Gollledge, N. R., McKay, R. M., Crampton, J. S., DeConto, R. M., De Santis, L., Florindo, F., Gasson, E. G. W., Harwood, D. M., Luyendyk, B. P., Powell, R. D., Clowes, C., and Kulhanek, D. K.: Antarctic ice-sheet sensitivity to obliquity forcing enhanced through ocean connections, *Nat. Geosci.*, 12, 132–137, <https://doi.org/10.1038/s41561-018-0284-4>, 2019.
- Livermore, R., Hillenbrand, C. D., Meredith, M., and Eagles, G.: Drake Passage and Cenozoic climate: an open and shut case?, *Geochem. Geophys. Geosy.*, 8, Q01005, <https://doi.org/10.1029/2005GC001224>, 2007.
- López-Quirós, A., Escutia, C., Etourneau, J., Rodríguez-Tovar, F. J., Bijl, P. K., Lobo, F. J., Bohoyo, F., Evangelinos, D., and Salabarnada, A.: Eocene–Miocene paleoceanographic changes in Drake Passage (Antarctica), POLAR 2018: Where the Poles come together. Abstract Proceedings, 487, WSL Institute for Snow and Avalanche Research SLF, ISBN 978-0-948277-54-2, 2018.
- López-Quirós, A., Escutia, C., Sánchez-Navas, A., Nieto, F., García-Casco, A., Martín-Algarra, A., Evangelinos, D., and Salabarnada, A.: Glaucony authigenesis, maturity and alteration in the Weddell Sea: An indicator of paleoenvironmental conditions before the onset of Antarctic glaciation, *Sci. Rep.*, 9, 1–12, 2019.
- López-Quirós, A., Sánchez-Navas, A., Nieto, F., and Escutia, C.: New insights into the nature of glauconite, *Am. Mineral.*, 105, 674–686, 2020.
- López-Quirós, A., Escutia, C., Etourneau, J., Rodríguez-Tovar, F. J., Roignant, S., Lobo, F. J., Thompson, N., Bijl, P. K., Bohoyo, F., and Salzmann, U.: Eocene–Oligocene paleoenvironmental changes in the South Orkney Microcontinent (Antarctica) linked to the opening of Powell Basin, *Glob. Planet. Change*, 204, 103581, <https://doi.org/10.1016/j.gloplacha.2021.103581>, 2021.
- Lyle, M., Gibbs, S., Moore, T. C., and Rea, D. K.: Late Oligocene initiation of the Antarctic Circumpolar Current: Evidence from the South Pacific, *Geology*, 35, 691–694, <https://doi.org/10.1130/g23806a.1>, 2007.
- Majewski, W. and Bohaty, S. M.: Surface-water cooling and salinity decrease during the Middle Miocene climate transition at Southern Ocean ODP Site 747 (Kerguelen Plateau), *Mar. Micropaleontol.*, 74, 1–14, 2010.
- Maldonado, A., Bohoyo, F., Galindo-Zaldívar, J., Hernández-Molina, J., Jabaloy, A., Lobo, F., Rodríguez-Fernández, J., Suriñach, E., and Vázquez, J.: Ocean basins near the Scotia–Antarctic plate boundary: influence of tectonics and paleoceanography on the Cenozoic deposits, *Mar. Geophys. Res.*, 27, 83–107, 2006.
- Maldonado, A., Bohoyo, F., Galindo-Zaldívar, J., Hernández-Molina, F. J., Lobo, F. J., Lodolo, E., Martos, Y. M., Pérez, L. F., Schreider, A. A., and Somoza, L.: A model of oceanic development by ridge jumping: opening of the Scotia Sea, *Glob. Planet. Change*, 123, 152–173, 2014.
- Marret, F., Bradley, L., de Vernal, A., Hardy, W., Kim, S.-Y., Mudie, P., Pénard, A., Pospelova, V., Price, A. M., and Radi, T.: From bi-polar to regional distribution of modern dinoflagellate cysts, an overview of their biogeography, *Mar. Micropaleontol.*, 159, 101753, <https://doi.org/10.1016/j.marmicro.2019.101753>, 2020.
- Marschalek, J., Zurli, L., Talarico, F., Van de Fliedert, T., Vermeesch, P., Carter, A., Beny, F., Bout-Roumazeilles, V., Sangiorgi, F., and Hemming, S.: A large West Antarctic Ice Sheet explains early Neogene sea-level amplitude, *Nature*, 600, 450–455, 2021.
- McKay, R., Barrett, P., Levy, R., Naish, T., Gollledge, N., and Pyne, A.: Antarctic Cenozoic climate history from sedimentary records: ANDRILL and beyond, *Philos. T. R. Soc. A*, 374, 20140301, <https://doi.org/10.1098/rsta.2014.0301>, 2016.
- McKay, R. M., De Santis, L., Kulhanek, D. K., Ash, J. L., Beny, F., Browne, I. M., Cortese, G., Cordeiro de Sousa, I. M., Dodd, J. P., Esper, O. M., Gales, J. A., Harwood, D. M., Ishino, S.,

- Keisling, B. A., Kim, S., Kim, S., Laberg, J. S., Leckie, R. M., Müller, J., Patterson, M. O., Romans, B. W., Romero, O. E., Sangiorgi, F., Seki, O., Shevenell, A. E., Singh, S. M., Sugisaki, S. T., van de Fliedert, T., van Peer, T. E., Xiao, W., and Xiong, Z.: Expedition 374 methods, in: Ross Sea West Antarctic Ice Sheet History, edited by: McKay, R. M., De Santis, L., Kulhanek, D. K., and the Expedition 374 Scientists, Proceedings of the International Ocean Discovery Program, 374: College Station, TX (International Ocean Discovery Program), <https://doi.org/10.14379/iodp.proc.374.102.2019>, 2019.
- Miller, K. G., Wright, J. D., and Browning, J. V.: Visions of ice sheets in a greenhouse world, *Mar. Geol.*, 217, 215–231, 2005.
- Müller, R. D., Cannon, J., Qin, X., Watson, R. J., Gurnis, M., Williams, S., Pfaffelmoser, T., Seton, M., Russell, S. H., and Zahirovic, S.: GPlates: building a virtual Earth through deep time, *Geochem. Geophys. Geosy.*, 19, 2243–2261, 2018.
- Neville, L. A., Grasby, S. E., and McNeil, D. H.: Limited freshwater cap in the Eocene Arctic Ocean, *Sci. Rep.*, 9, 4226, <https://doi.org/10.1038/s41598-019-40591-w>, 2019.
- Nicholson, U. and Stow, D.: Erosion and deposition beneath the Subantarctic Front since the Early Oligocene, *Sci. Rep.*, 9, 1–9, 2019.
- Orsi, A. H., Whitworth III, T., and Nowlin Jr, W. D.: On the meridional extent and fronts of the Antarctic Circumpolar Current, *Deep-Sea Res. Pt. I*, 42, 641–673, 1995.
- Parras, A., Guerin, G. R., Panera, J. P. P., Griffin, M., Nández, C., Cusiminsky, G., and Quiroga, A.: Integrated stratigraphy and paleontology of the lower Miocene Monte León Formation, southeastern Patagonia, Argentina: Unraveling paleoenvironmental changes and factors controlling sedimentation, *Palaeogeogr. Palaeoclimatol.*, 556, 109701, <https://doi.org/10.1016/j.palaeo.2020.109701>, 2020.
- Pérez, L. F., Hernández-Molina, F. J., Lodolo, E., Bohoyo, F., Galindo-Zaldívar, J., and Maldonado, A.: Oceanographic and climatic consequences of the tectonic evolution of the southern scotia sea basins, Antarctica, *Earth-Sci. Rev.*, 198, 102922, <https://doi.org/10.1016/j.earscirev.2019.102922>, 2019.
- Pérez, L. F., Martos, Y. M., García, M., Weber, M. E., Raymo, M. E., Williams, T., Bohoyo, F., Armbrrecht, L., Bailey, I., and Brachfeld, S.: Miocene to present oceanographic variability in the Scotia Sea and Antarctic ice sheets dynamics: Insight from revised seismic-stratigraphy following IODP Expedition 382, *Earth Planet. Sc. Lett.*, 553, 116657, <https://doi.org/10.1016/j.epsl.2020.116657>, 2021.
- Pérez, L. F., De Santis, L., McKay, R. M., Larter, R. D., Ash, J., Bart, P. J., Böhm, G., Brancatelli, G., Browne, I., and Colleoni, F.: Early and middle Miocene ice sheet dynamics in the Ross Sea: Results from integrated core-log-seismic interpretation, *GSA Bull.*, 134, 348–370, <https://doi.org/10.1130/B35814.1>, 2022.
- Plancq, J., Mattioli, E., Pittet, B., Simon, L., and Grossi, V.: Productivity and sea-surface temperature changes recorded during the late Eocene–early Oligocene at DSDP Site 511 (South Atlantic), *Palaeogeogr. Palaeoclimatol.*, 407, 34–44, 2014.
- Prebble, J. G., Crouch, E. M., Carter, L., Cortese, G., Bostock, H., and Neil, H.: An expanded modern dinoflagellate cyst dataset for the Southwest Pacific and Southern Hemisphere with environmental associations, *Mar. Micropaleontol.*, 101, 33–48, <https://doi.org/10.1016/j.marmicro.2013.04.004>, 2013.
- Premaor, E., Ferreira, E. P., Guerin, G. R., and Souza, P. A.: Eocene paleoceanographic and paleoclimatic events recognized by assemblages of dinoflagellate cysts in the Southwest Atlantic Ocean, *J. South Am. Earth Sci.*, 130, 104587, <https://doi.org/10.1016/j.jsames.2023.104587>, 2023.
- Pross, J. and Brinkhuis, H.: Organic-walled dinoflagellate cysts as paleoenvironmental indicators in the Paleogene; a synopsis of concepts, *Paläontol. Z.*, 79, 53–59, <https://doi.org/10.1007/BF03021753>, 2005.
- Reynolds, R. W., Rayner, N. A., Smith, T. M., Stokes, D. C., and Wang, W.: An improved in situ and satellite SST analysis for climate, *J. Clim.*, 15, 1609–1625, [https://doi.org/10.1175/1520-0442\(2002\)015<1609:AIISAS>2.0.CO;2](https://doi.org/10.1175/1520-0442(2002)015<1609:AIISAS>2.0.CO;2), 2002.
- Roberts, A. P., Bicknell, S. J., Byatt, J., Bohaty, S. M., Florindo, F., and Harwood, D. M.: Magnetostratigraphic calibration of Southern Ocean diatom datums from the Eocene-Oligocene of Kerguelen Plateau (Ocean Drilling Program sites 744 and 748), *Palaeogeogr. Palaeoclimatol.*, 198, 145–168, [doi.org/10.1016/S0031-0182\(03\)00397-3](https://doi.org/10.1016/S0031-0182(03)00397-3), 2023.
- Rohling, E. J., Foster, G. L., Gernon, T. M., Grant, K. M., Heslop, D., Hibbert, F. D., Roberts, A. P., and Yu, J.: Comparison and synthesis of sea-level and deep-sea temperature variations over the past 40 million years, *Rev. Geophys.*, 60, e2022RG000775, <https://doi.org/10.1029/2022RG000775>, 2022.
- Sangiorgi, F., Bijl, P. K., Passchier, S., Salzmann, U., Schouten, S., McKay, R., Cody, R. D., Pross, J., van de Fliedert, T., Bohaty, S. M., Levy, R., Williams, T., Escutia, C., and Brinkhuis, H.: Southern Ocean warming and Wilkes Land ice sheet retreat during the mid-Miocene, *Nat. Commun.*, 9, 317, <https://doi.org/10.1038/s41467-017-02609-7>, 2018.
- Sauermilch, I., Whittaker, J. M., Klocker, A., Munday, D. R., Hochmuth, K., Bijl, P. K., and LaCasce, J. H.: Gateway-driven weakening of ocean gyres leads to Southern Ocean cooling, *Nat. Commun.*, 12, 1–8, 2021.
- Scher, H. D., Whittaker, J. M., Williams, S. E., Latimer, J. C., Kordesch, W. E. C., and Delaney, M. L.: Onset of Antarctic Circumpolar Current 30 million years ago as Tasmanian Gateway aligned with westerlies, *Nature*, 523, 580–583, <https://doi.org/10.1038/nature14598>, 2015.
- Schreck, M. and Matthiessen, J.: *Batiacasphaera micropapillata*: Palaeobiogeographic distribution and palaeoecological implications of a critical Neogene species complex, *Biological and Geological Perspectives of Dinoflagellates*, The Micropalaeontological Society, Special Publications, Geol. Soc. Lond., 5, 301–314, 2013.
- Shevenell, A. E., Kennett, J. P., and Lea, D. W.: Middle Miocene ice sheet dynamics, deep-sea temperatures, and carbon cycling: A Southern Ocean perspective, *Geochem. Geophys. Geosy.*, 9, Q02006, <https://doi.org/10.1029/2007GC001736>, 2008.
- Sijp, W. P. and England, M. H.: Effect of the Drake Passage through-flow on global climate, *J. Phys. Oceanogr.*, 34, 1254–1266, 2004.
- Sijp, W. P., von der Heydt, A. S., and Bijl, P. K.: Model simulations of early westward flow across the Tasman Gateway during the early Eocene, *Clim. Past*, 12, 807–817, <https://doi.org/10.5194/cp-12-807-2016>, 2016.
- Sluijs, A., Brinkhuis, H., Stickley, C., Warnaar, J., Williams, G., and Fuller, M.: Dinoflagellate cysts from the Eocene/Oligocene transition in the Southern Ocean; results from ODP Leg 189, Pro-

- ceedings of the Ocean Drilling Program, *Sci. Res.*, 189, 1–42, <https://doi.org/10.2973/odp.proc.sr.189.104.2003>, 2003.
- Sluijs, A., Pross, J., and Brinkhuis, H.: From greenhouse to icehouse; organic-walled dinoflagellate cysts as paleoenvironmental indicators in the Paleogene, *Earth-Sci. Rev.*, 68, 281–315, 2005.
- Sluijs, A. and Brinkhuis, H.: A dynamic climate and ecosystem state during the Paleocene–Eocene Thermal Maximum: inferences from dinoflagellate cyst assemblages on the New Jersey Shelf, *Biogeosciences*, 6, 1755–1781, <https://doi.org/10.5194/bg-6-1755-2009>, 2009.
- Sosdian, S., Babila, T., Greenop, R., Foster, G., and Lear, C.: Ocean carbon storage across the middle Miocene: A new interpretation for the Monterey Event, *Nat. Commun.*, 11, 1–11, 2020.
- Stickley, C. E., Brinkhuis, H., Schellenberg, S. A., Sluijs, A., Röhl, U., Fuller, M., Grauert, M., Huber, M., Warnaar, J., and Williams, G. L.: Timing and nature of the deepening of the Tasmanian Gateway, *Paleoceanography*, 19, PA4027, <https://doi.org/10.1029/2004PA001022>, 2004.
- Stuart, K. and Long, D.: Tracking large tabular icebergs using the SeaWinds Ku-band microwave scatterometer, *Deep-Sea Res. Pt. II*, 58, 1285–1300, 2011.
- Thöle, L. M., Nooteboom, P. D., Hou, S., Wang, R., Nie, S., Michel, E., Sauermilch, I., Marret, F., Sangiorgi, F., and Bijl, P. K.: An expanded database of Southern Hemisphere surface sediment dinoflagellate cyst assemblages and their oceanographic affinities, *J. Micropalaeontol.*, 42, 35–56, <https://doi.org/10.5194/jm-42-35-2023>, 2023.
- Tibbitt, E. J., Warny, S., Tierney, J. E., Wellner, J. S., and Feakins, S. J.: Cenozoic Antarctic Peninsula Temperatures and Glacial Erosion Signals From a Multi-Proxy Biomarker Study, *Paleoceanogr. Paleocl.*, 37, e2022PA004430, <https://doi.org/10.1029/2022PA004430>, 2022.
- Toggweiler, J. R., Russell, J. L., and Carson, S. R.: Mid-latitude westerlies, atmospheric CO₂, and climate change during the ice ages, *Paleoceanography*, 21, PA2005, <https://doi.org/10.1029/2005PA001154>, 2006.
- Toumoulin, A., Donnadieu, Y., Ladant, J. B., Batenburg, S., Poblete, F., and Dupont-Nivet, G.: Quantifying the effect of the Drake Passage opening on the Eocene Ocean, *Paleoceanogr. Paleocl.*, 35, e2020PA003889, <https://doi.org/10.1029/2020PA003889>, 2020.
- van de Lagemaat, S. H., Swart, M. L., Vaes, B., Kusters, M. E., Boschman, L. M., Burton-Johnson, A., Bijl, P. K., Spakman, W., and van Hinsbergen, D. J.: Subduction initiation in the Scotia Sea region and opening of the Drake Passage: When and why?, *Earth-Sci. Rev.*, 215, 103551, <https://doi.org/10.1016/j.earscirev.2021.103551>, 2021.
- Verducci, M., Foresi, L., Scott, G., Sprovieri, M., Lirer, F., and Pelosi, N.: The Middle Miocene climatic transition in the Southern Ocean: evidence of paleoclimatic and hydrographic changes at Kerguelen plateau from planktonic foraminifers and stable isotopes, *Palaeogeogr. Palaeocl.*, 280, 371–386, 2009.
- Wall, D., Dale, B., Lohmann, G., and Smith, W. K.: The environmental and climatic distribution of dinoflagellate cysts in modern marine sediments from regions in the North and South Atlantic Oceans and adjacent seas, *Mar. Micropaleontol.*, 2, 121–200, 1977.
- Warnaar, J., Bijl, P. K., Huber, M., Sloan, L., Brinkhuis, H., Röhl, U., Sriver, R., and Visscher, H.: Orbitally forced climate changes in the Tasman sector during the Middle Eocene, *Palaeogeogr. Palaeoclimatol.*, 280, 361–370, 2009.
- Warny, S., Kymes, C. M., Askin, R. A., Krajewski, K. P., and Bart, P. J.: Remnants of Antarctic vegetation on King George Island during the early Miocene Melville glaciation, *Palynology*, 40, 66–82, <https://doi.org/10.1080/01916122.2014.999954>, 2016.
- Weber, M. E., Raymo, M. E., Peck, V. L., Williams, T., and the Expedition 382 Scientists: Site U1536, *Proceedings of the International Ocean Discovery Program*, Vol. 382, 2021.
- Williams, G. L., Fensome, R. A., and MacRae, R. A.: The Lentin and Williams Index of Fossil Dinoflagellates 2017 Edition, <https://palynology.org/wp-content/uploads/2017/01/AASP-Contribution-Series-No.48.pdf> (last access: 18 November 2023), 2017.
- Zonneveld, K. A. F., Versteegh, G. J. M., Kasten, S., Eglinton, T. I., Emeis, K.-C., Huguet, C., Koch, B. P., de Lange, G. J., de Leeuw, J. W., Middelburg, J. J., Mollenhauer, G., Prahl, F. G., Rethemeyer, J., and Wakeham, S. G.: Selective preservation of organic matter in marine environments; processes and impact on the sedimentary record, *Biogeosciences*, 7, 483–511, <https://doi.org/10.5194/bg-7-483-2010>, 2010.
- Zonneveld, K. A., Marret, F., Versteegh, G. J., Bogus, K., Bonnet, S., Bouimetarhan, I., Crouch, E., de Vernal, A., Elshaniawany, R., and Edwards, L.: Atlas of modern dinoflagellate cyst distribution based on 2405 data points, *Rev. Palaeobot. Palynol.*, 191, 1–197, <https://doi.org/10.1016/j.revpalbo.2012.08.003>, 2013.